



Cite this: DOI: 10.1039/d0nj03774e

# Design, synthesis, molecular simulation, and biological activities of novel quinazolinone-pyrimidine hybrid derivatives as dipeptidyl peptidase-4 inhibitors and anticancer agents†

 Leila Emami,<sup>a</sup> Zahra Faghhi,<sup>b</sup> Amirhossein Sakhteman,<sup>a</sup> Zahra Rezaei,<sup>ac</sup> Zeinab Faghhi,<sup>c</sup> Farnaz Salehi<sup>a</sup> and Soghra Khabnadideh  <sup>\*ac</sup>

Two novel series of quinazolinone-pyrimidine (series a: **9a–9i**) and benzyl-pyrimidine hybrids (series b: **12a–12c**) were designed, synthesized and characterized by spectroscopic methods. The dipeptidyl peptidase-4 inhibition potencies of these compounds were assessed through a MAK 203 kit. Compound **9e** was found to be the most potent agent with an  $IC_{50}$  value of  $34.3 \pm 3.3 \mu\text{M}$ . A kinetic study revealed that it acted as a competitive inhibitor. Molecular modeling of these compounds was in agreement with the *in vitro* results. Due to the crucial role of dipeptidyl peptidase-4 in cancer therapy, the cytotoxic activities of the compounds were also evaluated against three cancerous cell lines (HT-29, SW1116 and A549). Almost all the compounds displayed better antiproliferative activity on colon cancer cell lines (HT-29 and SW1116) compared to a lung cancer cell line (A549). Compounds **9e** and **12c** exhibited significant activity toward the HT-29 cell line with an  $IC_{50}$  of  $10.67 \pm 0.3 \mu\text{M}$  and  $27.9 \pm 6.5 \mu\text{M}$  in comparison to sitagliptin and cisplatin as a positive control, respectively. Among the different cells, the compounds showed the best inhibitory effects on HT-29, which was compatible with the greater expression of the dipeptidyl peptidase-4 marker detected by flow cytometry in this cell line. Further studies on the hit compounds (**9e** and **12c**) through cell cycle and apoptosis assays also showed that these compounds could induce cell death by apoptosis or arrest cells in the G2/M phase. Accordingly, the results imply that **9e** is a potent inhibitor of dipeptidyl peptidase-4 with efficient anti-cancer activity and could play a role as a cytotoxic agent in colorectal cancer.

 Received 27th July 2020,  
 Accepted 17th October 2020

DOI: 10.1039/d0nj03774e

[rsc.li/njc](http://rsc.li/njc)

## 1. Introduction

Dipeptidyl peptidase-4 (DPP-4), also identified as Cluster of Differentiation 26 (CD26), is a glycoprotein with enzyme activity expressed in different tissue and cell types. Its exopeptidase function regulates the activity of a variety of substrates, for instance cytokines, growth factors, neuropeptides, and incretin hormones such as glucagon-like peptide-1 (GLP-1) and GLP-2.<sup>1–3</sup> Consequently, DPP-4 (CD26) is currently considered as a target of great importance in the treatment of various disorders in particular diabetes mellitus type 2 (DM-2) and cancer. Recently,

DPP-4 (CD26) inhibitors have been applied as oral hypoglycemic drugs with excellent safety profiles and minimal side effects. By inhibiting the DPP-4 transmembrane glycoprotein enzyme, these drugs retain glucose homeostasis at the desired value with an increase in the release of insulin and a decrease in glucagon secretion and gluconeogenesis.<sup>4,5</sup> Six FDA approved DPP-4 inhibitors including sitagliptin (2006), vildagliptin (2007), saxagliptin (2009), alogliptin (2010), linagliptin (2011) and teneligliptin (2012) are available currently for DM-2 treatment. On the other hand, recently, the role of DPP-4 inhibitors in cancer treatment has been a topic of interest in the research area. They play a crucial role in cancer as tumor suppressors or activators depending on their level of expression and interaction with the microenvironment and selected chemokines.<sup>6–8</sup> On top of that it has been revealed that DPP-4 inhibition in colorectal and lung cancers is associated with improved overall survival of the patients, probably due to interacting with immune cells through chemokines, leading to their degradation.<sup>9</sup> In a mouse model of hepatocellular carcinoma, DPP-4 inhibitors could also clinically inhibit the progression of cancer or augment the anti-tumor effects of molecular-targeting

<sup>a</sup> Department of Medicinal Chemistry, School of Pharmacy, Shiraz University of Medical Sciences, Shiraz, Iran. E-mail: khabns@sums.ac.ir; Fax: +98-71-32424126; Tel: +98-71-32424127-8

<sup>b</sup> Shiraz Institute for Cancer Research, Medical School, Shiraz University of Medical Sciences, Shiraz, Iran

<sup>c</sup> Pharmaceutical Sciences Research Center, Shiraz University of Medical Sciences, Shiraz, Iran

† Electronic supplementary information (ESI) available. See DOI: 10.1039/d0nj03774e

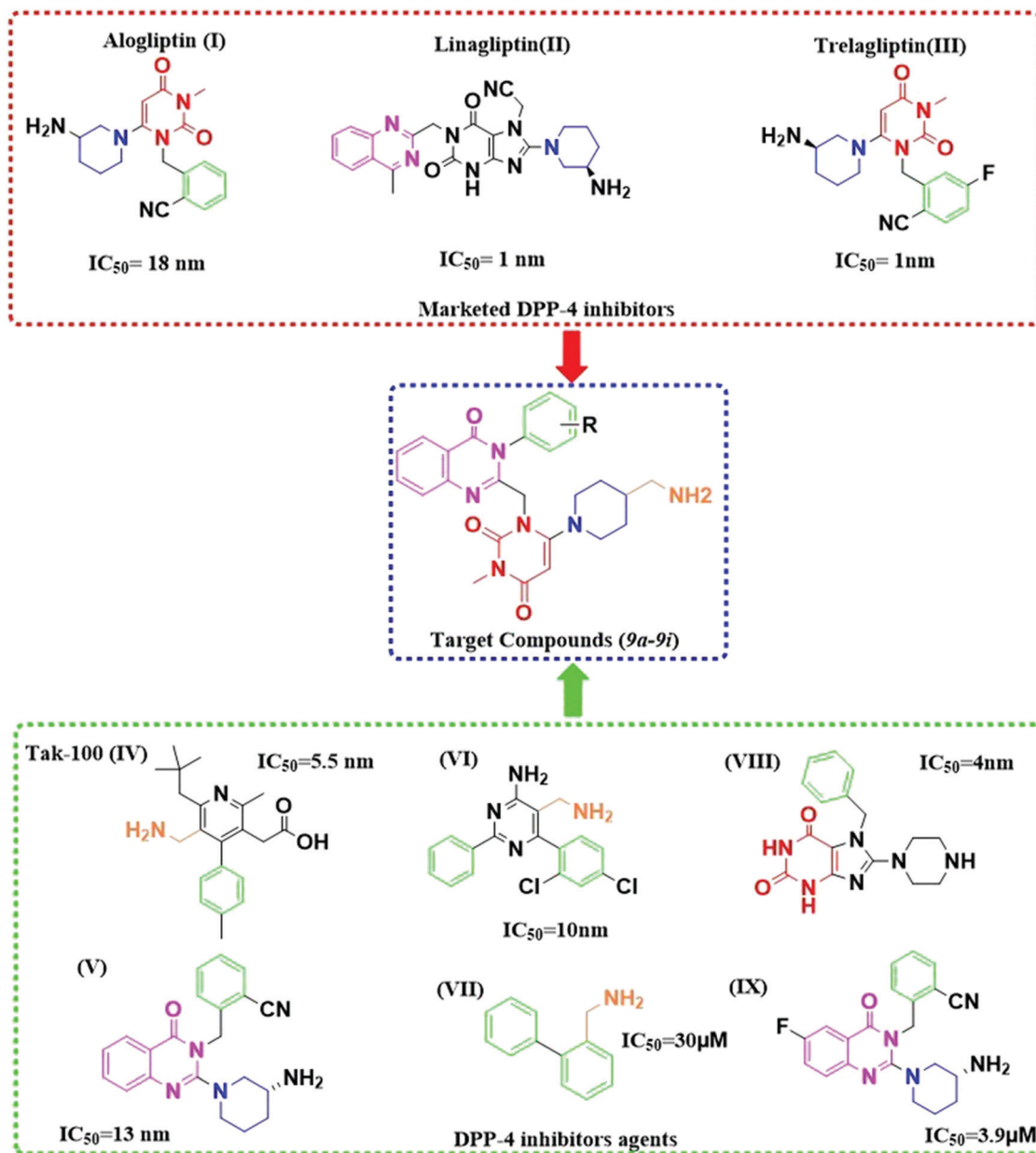


Fig. 1 Molecular hybridization design of 3-methyl-6-chloro-uracil-2-chloromethyl-3-substituted phenylquinazolin-4(3H)-one bearing 4-(amino-methyl) piperidine as novel DPP-4 inhibitory agents.

drugs or immunotherapies.<sup>10</sup> It has been also shown that sitagliptin limits tumor growth by enhancing chemokine mediated eosinophil migration. DPP-4 (CD26) can also regulate the expression of matrix metalloproteinase, which is responsible for destroying the extracellular matrix, a necessary process for cancer attack and metastasis.<sup>11–13</sup>

Quinazoline and quinazolinone are considered as favorable and significant medical scaffolds that possess a variety of pharmacological properties including antidiabetic,<sup>14–17</sup> anticancer,<sup>18–22</sup> antifungal,<sup>23–25</sup> antibacterial<sup>26–28</sup> and antihypertensive activity.<sup>29</sup> Besides, there is a great deal of evidence showing pyrimidine analogs as DPP-4 inhibitors.<sup>30–32</sup> Thus, in the present study, for the design of new target compounds with DPP-4

inhibitory activity, we focused on two parameters: firstly, the structures of alogliptin (I) ( $IC_{50} < 10$  nM), linagliptin (II) ( $IC_{50} < 1$  nM), and trelagliptin (III) ( $IC_{50} < 1$  nM) as three main potent and selective DPP-4 inhibitors on the market, and, secondly, various quinazolinone and pyrimidine scaffolds, which have been proved to be useful as DPP-4 inhibitory agents (structures IV–IX) (Fig. 1).<sup>33–38</sup> Accordingly, a pharmacophore approach was performed to obtain a hybrid structure of aminomethyl piperidine-pyrimidines with or without quinazolinone. Herein, in order to increase the DPP-4 inhibition potencies and to give more diversity, a 3-substituted phenyl moiety was also substituted on the quinazolinone ring. This substitution was considered to improve the interactions, *i.e.*, electronic and hydrophobic, with

the enzyme. Furthermore, we replaced the (3R)-aminopiperidine group of structures V and IX (Fig. 1) with pyrimidine substituted with a 4-(aminomethyl) piperidine moiety, which is expected to interact with the DPP-4 enzyme active site through salt bridges as the critical hydrogen bonding interactions. The binding mode of the novel designed compounds was then evaluated with computational docking studies on the DPP-4 receptor (PDB code: 4a5s). Molecular docking simulations were then performed on two potent compounds (**9e** and **9f**) to reach a full molecular binding mode interacting with the key amino acids in the active site of the DPP-4 enzyme in the steady state. Pharmacological evaluations of the designed compounds as DPP-4 inhibitors were also performed using a MAK 203 kit. Moreover, the cytotoxic effect of the new compounds with DPP-4 inhibitory activities was assessed against human cancerous cell lines as well as normal cell lines. Additionally, the induction of apoptosis and cell cycle analysis were done to investigate the antiproliferative activity and mechanism of the cytotoxic effect on the colon cancer cell lines.

## 2. Experimental

### 2.1. Chemistry

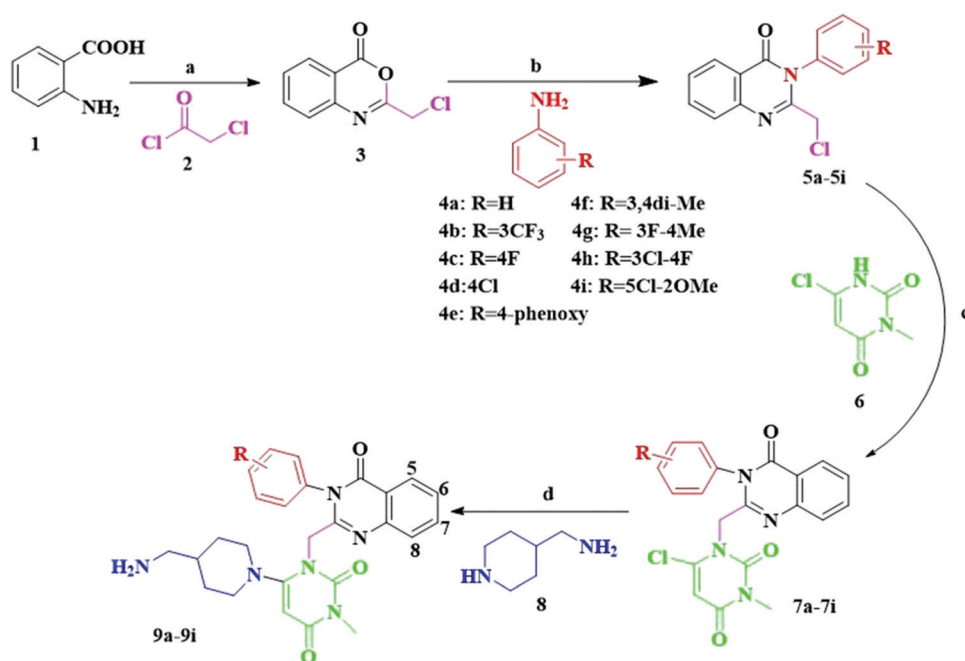
All chemicals and solvents were obtained from the Sigma Aldrich, Merck, and Samchun companies without any purification. Silica gel pre-coated analytical thin-layer chromatography (TLC) plates were used for monitoring the reaction progress. Melting points were obtained on an Electrothermal 9200 apparatus (Electrothermal, UK), and infrared spectra were determined on a VERTEX70 spectrometer (Bruker, Germany).  $^1\text{H}$  NMR and

$^{13}\text{C}$  NMR spectra were recorded using a BRUKER DRX-AVANCE 400 MHz and 100 MHz, respectively, in  $\text{DMSO-d}_6$ . Mass spectra were recorded on a mass instrument using the (M+1) mode from Agilent (Agilent Technologies, USA).

**2.1.1. General procedure for the synthesis of 2-(chloromethyl)-4H-benzo[d][1,3]oxazin-4-one (3).** To a solution of anthranilic acid (**1**) (1 mmol) in dichloromethane (10 mL), diisopropylethylamine (DIPEA) (1.5 mmol) was added. Then 1.2 mmol of chloroacetyl chloride (**2**) was added dropwise for 20 minutes at room temperature, and the reaction mixture was stirred for 2 hours. The reaction mixture was washed with water and extracted with ethyl acetate ( $2 \times 20$  mL) and the organic layers dried with anhydrous  $\text{Na}_2\text{SO}_4$ . Then the remaining solvents were evaporated in a vacuum to obtain the product (Scheme 1, step a).

**2.1.2. General procedure for the synthesis of 2-(chloromethyl)-3-substituted quinazolin-4(3H)-one (5a–5i).** Intermediate **3** was treated with different substituted anilines (**4a–4i**) (1 mmol) and  $\text{PCl}_3$  (1.5 mmol) in acetonitrile ( $\text{CH}_3\text{CN}$ ) at  $60^\circ\text{C}$  for 2 hours. After completion of the reaction, a saturated  $\text{NaHCO}_3$  solution was added and extracted with ethyl acetate ( $3 \times 20$  mL). The organic layers were dried with anhydrous  $\text{Na}_2\text{SO}_4$ , and the crude products were purified by recrystallization with ethanol (Scheme 1, step b).

**2.1.3. General procedure for the synthesis of 6-chloro-3-methyl-2-((4-oxo-3-phenyl-3,4-dihydroquinazolin-2-yl) methyl) pyrimidine-2,4(1H,3H)-dione derivatives (7a–7i).** 6-Chloro-3-methyl uracil (**6**) (2 mmol) was added to the different derivatives of intermediates **5a–5i** (2 mmol) in acetonitrile with the presence of DIPEA (1.5 mmol). The mixture was stirred under reflux conditions for 24 hours. After completion of the reaction, the solvent was



**Scheme 1** Synthesis of the amino-quinazolinone-pyrimidine hybrids (**9a–9i**). Reagents and conditions: (a) DIPEA, DCM, r.t., 2 h. (b) MeCN,  $\text{PCl}_3$ ,  $60^\circ\text{C}$ , 2 h. (c) DIPEA, MeCN, reflux, 24 h. (d) i-PrOH,  $\text{NaHCO}_3$ ,  $65^\circ\text{C}$ , 24 h.

evaporated and purified by column chromatography using chloroform/*n*-hexane (25/75) as an eluent (Scheme 1, step c).

**2.1.4. General procedure for the synthesis of 6-(4-(aminomethyl) piperidine-1-yl)-3-substituted-1-((4-oxo-3-phenyl-3,4-dihydroquinazolin-2-yl) methyl) pyrimidine-2,4(1H,3H)-dione derivatives (9a–9i).** 4-(Aminomethyl) piperidine (**8**) (0.55 mmol) was added to compounds **7a–7i** (0.5 mmol) in isopropanol (10 mL) and sodium bicarbonate (2.02 mmol) at room temperature. The reaction mixture was warmed to 65 °C and heated for 24 hours. After completion of the reaction, the solvent was removed and extracted with dichloromethane (3 × 30 mL). Then the solvent was removed and recrystallized from a mixture of dichloromethane and *n*-hexane to achieve the final products (Scheme 1, step d).

**2.1.4.1 6-(4-(Aminomethyl) piperidin-1-yl)-3-methyl-1-((4-oxo-3-phenyl-3,4-dihydroquinazolin-2-yl) methyl) pyrimidine-2,4(1H,3H)-dione (9a).** Yellow solid; yield 69%; m.p. 184 °C; IR (KBr, cm<sup>-1</sup>): 3431 (NH<sub>2</sub>), 3365 (NH<sub>2</sub>), 2924 (CH), 2853 (CH), 1686 (C=O), 1660 (C=O), 1611 (C=O), 1593 (C=N), 1473 (C=C), 1333 (C-N), 1271–1193 (C-O). <sup>1</sup>H NMR (400 MHz, DMSO-d<sub>6</sub>) δ<sub>H</sub> (ppm): 7.907 (d, 1H, *J* = 7.6 Hz, H-5-quinazolinone), 7.622–7.663 (m, 1H, H-7-quinazolinone), 7.459 (d, 1H, *J* = 8 Hz, H-8-quinazolinone), 7.336–7.368 (m, 1H, H-6-quinazolinone), 7.273–7.331 (m, 3H, aromatic), 7.229 (d, 2H, *J* = 6.4 Hz, aromatic), 4.867 (s, 2H, quinazolinone-CH<sub>2</sub>), 4.813 (s, 1H, uracil), 3.742 (d, 2H, *J* = 14 Hz, NH<sub>2</sub>), 2.881 (s, 3H, CH<sub>3</sub>-uracil), 2.377–2.436 (m, 2H, aliphatic), 2.198 (d, 2H, *J* = 6.4 Hz, piperidine-CH<sub>2</sub>-NH<sub>2</sub>), 1.273–1.374 (m, 3H, aliphatic), 0.928–1.035 (m, 1H, aliphatic), 0.616–0.679 (m, 3H, aliphatic). <sup>13</sup>C NMR (100 MHz, DMSO-d<sub>6</sub>) δ<sub>C</sub> (ppm): 162.47, 160.99, 158.93, 154.35, 151.05, 146.69, 135.73, 134.91, 129.47, 129.34, 128.36, 127.43, 127.3, 126.42, 120.87, 79.25, 65.98, 45.08, 43.91, 36.71, 28.59, 26.56. MS (*m/z*, %): 472.5 (M<sup>+</sup>, 11.25), 442.5 (21.25), 393.5 (5.1), 358.5 (57), 149.1 (11.25), 112.2 (2.5), 80.0 (67.5), 71.1 (51.2), 48.1 (100). Elem. anal. calcd. for C<sub>26</sub>H<sub>28</sub>N<sub>6</sub>O<sub>3</sub> (472.5); C, 66.09; H, 5.97; N, 17.78. Found: C, 66.02; H, 5.62; N, 17.71.

**2.1.4.2 6-(4-(Aminomethyl) piperidin-1-yl)-3-methyl-1-((4-oxo-3-(3-(trifluoromethyl) phenyl)-3,4-dihydroquinazolin-2-yl) methyl) pyrimidine-2,4(1H,3H)-dione (9b).** Cream powder; yield 78%; m.p. 173–176 °C; IR (KBr, cm<sup>-1</sup>): 3442 (NH<sub>2</sub>), 3386 (NH<sub>2</sub>), 2927 (CH), 2852 (CH), 1696 (C=O), 1661 (C=O), 1595 (C=O), 1548 (C=N), 1475 (C=C), 1308 (C-N), 1261–1170 (C-O), 1071 (C-F). <sup>1</sup>H NMR (400 MHz, DMSO-d<sub>6</sub>) δ<sub>H</sub> (ppm): 8.168 (d, 1H, *J* = 8 Hz, H-5-quinazolinone), 7.999 (s, 1H, aromatic), 7.924 (td, 1H, *J* = 8.4 Hz, *J* = 1.2 Hz, H-7-quinazolinone), 7.864 (s, 2H, aromatic), 7.801 (d, 1H, *J* = 8 Hz, aromatic), 7.755 (d, 1H, *J* = 8 Hz, aromatic), 7.627 (t, 1H, *J* = 7.6 Hz, aromatic), 5.071–5.228 (m, 2H, quinazolinone-CH<sub>2</sub>), 5.033 (s, 1H, uracil), 3.983 (d, 2H, *J* = 11.2 Hz, NH<sub>2</sub>), 3.062 (s, 3H, CH<sub>3</sub>-uracil), 2.608–2.669 (m, 2H, aliphatic), 2.355 (d, 2H, *J* = 6.4 Hz, piperidine-CH<sub>2</sub>-NH<sub>2</sub>), 1.528–1.599 (m, 2H, aliphatic), 1.399–1.467 (m, 1H, aliphatic), 1.174–1.273 (m, 2H, aliphatic), 0.868–0.817 (m, 2H, aliphatic). <sup>13</sup>C NMR (100 MHz, DMSO-d<sub>6</sub>) δ<sub>C</sub> (ppm): 162.37, 161.11, 158.85, 154.04, 150.53, 146.64, 136.73, 135.06, 132.95, 130.70, 127.66, 127.39, 126.42, 126.12, 125.67,

125.63, 120.90, 79.13, 66.39, 47.11, 44.15, 38.515, 28.85, 26.40. MS (*m/z*, %): 540.4 (M<sup>+</sup>, 3.2), 459.2 (1.1), 415.3 (2.2), 332 (6.97), 303.2 (54.35), 289.1 (38), 234.1 (10.5), 200 (10.38), 145.1 (100), 90.1 (62.4), 68.1 (50.39), 50.1 (32.01). Elem. anal. calcd. for C<sub>27</sub>H<sub>27</sub>F<sub>3</sub>N<sub>6</sub>O<sub>3</sub> (540.5); C, 59.99; H, 5.03; N, 15.55. Found: C, 59.86; H, 5.06; N, 15.62.

**2.1.4.3 6-(4-(Aminomethyl) piperidin-1-yl)-1-((3-(4-fluorophenyl)-4-oxo-3,4-dihydroquinazolin-2-yl) methyl)-3-methyl pyrimidine-2,4(1H,3H)-dione (9c).** White powder; yield 83%; m.p. 156–160 °C; IR (KBr, cm<sup>-1</sup>): 3447 (NH<sub>2</sub>), 3370 (NH<sub>2</sub>), 2925 (CH), 2854 (CH), 1698 (C=O), 1676 (C=O), 1609 (C=O), 1550 (C=N), 1471 (C=C), 1370 (C-N), 1224–1158 (C-O), 1114 (C-F). <sup>1</sup>H NMR (500 MHz, DMSO-d<sub>6</sub>) δ<sub>H</sub> (ppm): 8.154 (d, 1H, *J* = 7.6 Hz, H-5-quinazolinone), 7.899 (td, 1H, *J* = 8 Hz, *J* = 1.2 Hz, H-7-quinazolinone), 7.719 (d, 1H, *J* = 8 Hz, H-8-quinazolinone), 7.604 (t, 1H, *J* = 8 Hz, H-6-quinazolinone), 7.537–7.571 (m, 2H, aromatic), 7.387 (t, 2H, *J* = 8.8 Hz, aromatic), 5.138 (s, 2H, quinazolinone-CH<sub>2</sub>), 5.049 (s, 1H, uracil), 3.993 (d, 2H, *J* = 10.8 Hz, NH<sub>2</sub>), 3.134 (s, 3H, CH<sub>3</sub>-uracil), 2.654 (t, 2H, *J* = 12.4 Hz, aliphatic), 2.333 (d, 2H, *J* = 6.4 Hz, piperidine-CH<sub>2</sub>-NH<sub>2</sub>), 1.545–1.606 (m, 2H, aliphatic), 1.339–1.469 (m, 1H, aliphatic), 1.174–1.30 (m, 1H, aliphatic), 0.835–0.883 (m, 3H, aliphatic). <sup>13</sup>C NMR (125 MHz, DMSO-d<sub>6</sub>) δ<sub>C</sub> (ppm): 163.36, 162.45, 161.13, 158.89, 154.25, 151.03, 146.66, 134.95, 131.98, 130.77, 130.69, 127.52, 127.33, 126.42, 120.88, 116.46, 116.23, 79.11, 66.15, 47.21, 44.19, 38.69, 28.84, 26.56. MS (*m/z*, %): 490.4 (M<sup>+</sup>, 8.9), 473.4 (9.4), 461.3 (5.2), 376.3 (2.1), 361.3 (3.7), 280.2 (3.6), 269.1 (76.3), 254.2 (83.11), 239.2 (100), 212.2 (10.12), 143.2 (19.45), 119.2 (30.46), 95.1 (66.48). Elem. anal. calcd. for C<sub>26</sub>H<sub>27</sub>FN<sub>6</sub>O<sub>3</sub> (490.5); C, 63.66; H, 5.55; N, 17.13. Found: C, 63.61; H, 5.58; N, 17.15.

**2.1.4.4 6-(4-(Aminomethyl) piperidin-1-yl)-1-((3-(4-chlorophenyl)-4-oxo-3,4-dihydroquinazolin-2-yl) methyl)-3-methylpyrimidine-2,4(1H,3H)-dione (9d).** Cream powder; yield 76%; m.p. 86–91 °C; IR (KBr, cm<sup>-1</sup>): 3445 (NH<sub>2</sub>), 3387 (NH<sub>2</sub>), 2922 (CH), 2850 (CH), 1686 (C=O), 1607 (C=O), 1490 (C=N), 1473 (C=C), 1384 (C-N), 1271–1185 (C-O), 865 (C-Cl). <sup>1</sup>H NMR (400 MHz, DMSO-d<sub>6</sub>) δ<sub>H</sub> (ppm): 8.201 (d, 1H, *J* = 8 Hz, H-5-quinazolinone), 7.924 (t, 1H, *J* = 8 Hz, H-7-quinazolinone), 7.753 (s, 1H, aromatic), 7.732 (s, 1H, aromatic), 7.611–7.633 (m, 4H, aromatic), 5.331 (s, 1H, uracil), 4.753 (s, 2H, quinazolinone-CH<sub>2</sub>), 3.605 (d, 2H, *J* = 7.2 Hz, NH<sub>2</sub>), 3.148 (s, 3H, CH<sub>3</sub>-uracil), 2.468 (d, 2H, *J* = 6.4 Hz, piperidine-H-NH<sub>2</sub>), 1.718 (d, 2H, *J* = 11.6 Hz aliphatic), 1.480–1.589 (m, 1H, aliphatic), 1.314–1.382 (m, 2H, aliphatic), 1.119–1.172 (m, 3H, aliphatic), 0.916–0.958 (m, 1H, aliphatic). <sup>13</sup>C NMR (100 MHz, DMSO-d<sub>6</sub>) δ<sub>C</sub> (ppm): 162.15, 161.06, 159.93, 152.05, 151.91, 146.63, 134.97, 134.68, 134.10, 130.23, 129.76, 127.09, 126.41, 121.04, 120.40, 88.66, 50.71, 47.13, 46.98, 38.21, 28.79, 27.21. MS (*m/z*, %): 507.2 (M<sup>+</sup>, 6.1), 469.4 (44.7), 438.3 (3.5), 392.3 (79.45), 335.2 (56.18), 304.1 (42.3), 269.1 (50.9), 255.1 (100), 234.2 (14.44), 165.1 (33.77), 143.1 (39.17), 111.1 (44.15), 75.1 (30.03). Elem. anal. calcd. for C<sub>26</sub>H<sub>27</sub>ClN<sub>6</sub>O<sub>3</sub> (506.1); C, 61.6; H, 5.37; N, 16.58. Found: C, 61.9; H, 5.31; N, 16.64.

**2.1.4.5 6-(4-(Aminomethyl) piperidin-1-yl)-3-methyl-1-((4-oxo-3-(4-phenoxy phenyl)-3,4-dihydro quinazolin-2-yl) methyl) pyrimidine-2,4(1H,3H)-dione (9e).** Cream powder; yield 87%; m.p. 116–119 °C; IR (KBr,  $\text{cm}^{-1}$ ): 3441 ( $\text{NH}_2$ ), 3385 ( $\text{NH}_2$ ), 2922 (CH), 2850 (CH), 1665 (C=O), 1601 (C=O), 1504 (C=N), 1473 (C=C), 1240 (C-N), 1185–1164 (C-O).  $^1\text{H}$  NMR (400 MHz,  $\text{DMSO-d}_6$ )  $\delta_{\text{H}}$  (ppm): 7.92 (dd, 1H,  $J = 8$  Hz,  $J = 1.2$  Hz, H-5-quinazolinone), 7.652 (t, 1H,  $J = 8$  Hz, H-7-quinazolinone), 7.477 (d, 1H,  $J = 8$  Hz, H-8-quinazolinone), 7.36 (t, 1H,  $J = 7.2$  Hz, H-6-quinazolinone), 7.186–7.253 (m, 4H, aromatic), 6.973 (t, 1H,  $J = 7.2$  Hz, aromatic), 6.861 (d, 2H,  $J = 8.8$  Hz, aromatic), 6.809 (d, 2H,  $J = 7.6$  Hz, aromatic), 4.932 (s, 2H, quinazolinone- $\text{CH}_2$ ), 4.860 (s, 1H, uracil), 3.779 (d, 2H,  $J = 11.2$  Hz,  $\text{NH}_2$ ), 2.901 (s, 3H,  $\text{CH}_3$ -uracil), 2.419 (t, 2H,  $J = 12$  Hz, aliphatic), 2.053 (d, 2H,  $J = 6.4$  Hz, piperidine- $\text{CH}_2$ - $\text{NH}_2$ ), 1.337 (d, 2H,  $J = 11.2$  Hz, aliphatic), 1.120–1.199 (m, 1H, aliphatic), 0.987 (d, 1H,  $J = 8$  Hz, aliphatic), 0.618–0.574 (m, 3H, aliphatic).  $^{13}\text{C}$  NMR (100 MHz,  $\text{DMSO-d}_6$ )  $\delta_{\text{C}}$  (ppm): 162.49, 161.17, 158.94, 157.38, 155.76, 154.24, 151.19, 146.65, 134.89, 130.49, 130.22, 130.15, 127.49, 127.32, 126.42, 124.15, 120.91, 119.19, 118.58, 79.17, 66.28, 47.19, 44.24, 38.679, 28.84, 26.59. MS ( $m/z$ , %): 564.4 ( $\text{M}^+$ , 1.2), 525.3 (3.1), 362.2 (8.3), 343.2 (48.65), 328.2 (100), 313.2 (52), 237.2 (62.1), 234.1 (30.5), 143.1 (29.1), 115.1 (23.86), 77.1 (70.17). Elem. anal. calcd. for  $\text{C}_{32}\text{H}_{32}\text{N}_6\text{O}_4$  (564.65); C, 68.07; H, 5.71; N, 14.88. Found: C, 68.13; H, 5.68; N, 14.89.

**2.1.4.6 6-(4-(Amino methyl) piperidin-1-yl)-1-((3-(3,4-dimethyl phenyl)-4-oxo-3,4-dihydro quinazolin-2-yl) methyl)-3-methyl pyrimidine-2,4(1H,3H)-dione (9f).** White powder; yield 87%; m.p. 178 °C; IR (KBr,  $\text{cm}^{-1}$ ): 3446 ( $\text{NH}_2$ ), 3386 ( $\text{NH}_2$ ), 2922 (CH), 2852 (CH), 1687 (C=O), 1661 (C=O), 1598 (C=O), 1548 (C=N), 1457 (C=C), 1272 (C-N), 1272–1191 (C-O).  $^1\text{H}$  NMR (300 MHz,  $\text{DMSO-d}_6$ )  $\delta_{\text{H}}$  (ppm): 8.137 (d, 1H,  $J = 7.5$  Hz, H-5-quinazolinone), 7.872 (t, 1H,  $J = 7.2$  Hz, H-7-quinazolinone), 7.698 (d, 1H,  $J = 7.8$  Hz, H-8-quinazolinone), 7.579 (t, 1H,  $J = 7.2$  Hz, H-6-quinazolinone), 7.260–7.285 (m, 1H, aromatic), 7.190–7.135 (m, 2H, aromatic), 5.285 (d, 1H,  $J = 13.8$  Hz, uracil), 4.987–5.036 (m, 2H, quinazolinone- $\text{CH}_2$ ), 3.974 (d, 2H,  $J = 9.6$  Hz,  $\text{NH}_2$ ), 3.126 (s, 3H,  $\text{CH}_3$ -uracil), 2.60–2.674 (m, 2H, aliphatic), 2.389 (d, 2H,  $J = 5.4$  Hz, piperidine- $\text{CH}_2$ - $\text{NH}_2$ ), 2.237 (s, 3H,  $\text{CH}_3$ -aromatic), 2.179 (s, 3H,  $\text{CH}_3$ -aromatic), 1.472–1.594 (m, 3H, aliphatic), 1.186–1.270 (m, 1H, aliphatic), 0.866 (s, 3H, aliphatic).  $^{13}\text{C}$  NMR (75 MHz,  $\text{DMSO-d}_6$ )  $\delta_{\text{C}}$  (ppm): 162.99, 161.55, 159.31, 154.68, 151.80, 147.17, 138.12, 138.06, 135.31, 133.69, 130.81, 129.37, 127.92, 127.79, 126.87, 125.84, 121.40, 79.46, 66.52, 47.02, 44.45, 38.27, 29.30, 26.94, 19.66, 19.53. MS ( $m/z$ , %): 369.3 (15.57), 249.2 (1.89), 196.2 (10.92), 173.2 (100), 103.1 (4.78), 77.2 (28.35), 51.2 (6.24). Elem. anal. calcd. for  $\text{C}_{28}\text{H}_{32}\text{N}_6\text{O}_3$  (500.6); C, 67.18; H, 6.44; N, 16.79. Found: C, 67.21; H, 6.12; N, 16.82.

**2.1.4.7 6-(4-(Amino methyl) piperidin-1-yl)-1-((3-(3-fluoro-4-methyl phenyl)-4-oxo-3,4-dihydro quinazolin-2-yl) methyl)-3-methyl pyrimidine-2,4(1H,3H)-dione (9g).** White powder; yield 72%; m.p. 145–150 °C; IR (KBr,  $\text{cm}^{-1}$ ): 3447 ( $\text{NH}_2$ ), 3386 ( $\text{NH}_2$ ), 3003–3037 (CH), 2927–2850 (CH), 1690 (C=O), 1661

(C=O), 1607 (C=O), 1549 (C=N), 1506 (C=C), 1332 (C-N), 1275–1193 (C-O).  $^1\text{H}$  NMR (400 MHz,  $\text{DMSO-d}_6$ )  $\delta_{\text{H}}$  (ppm): 8.158 (d, 1H,  $J = 7.2$  Hz, H-5-quinazolinone), 7.904 (t, 1H,  $J = 7.2$  Hz, H-7-quinazolinone), 7.729 (d, 1H,  $J = 8$  Hz, aromatic), 7.610 (t, 1H,  $J = 7.2$  Hz, aromatic), 7.383–7.424 (m, 2H, aromatic), 7.218 (d, 1H,  $J = 8$  Hz, aromatic), 5.196 (s, 2H, quinazolinone- $\text{CH}_2$ ), 5.044 (s, 1H, uracil), 4.001 (d, 2H,  $J = 10.4$  Hz,  $\text{NH}_2$ ), 3.126 (s, 3H,  $\text{CH}_3$ -uracil), 2.654 (t, 2H,  $J = 12.4$  Hz, aliphatic), 2.355 (d, 2H,  $J = 6$  Hz, piperidine- $\text{CH}_2$ - $\text{NH}_2$ ), 2.263 (s, 3H,  $\text{CH}_3$ -aromatic), 1.556–1.730 (m, 3H, aliphatic), 1.401–1.424 (m, 1H, aliphatic), 0.785–1.05 (m, 3H, aliphatic).  $^{13}\text{C}$  NMR (100 MHz,  $\text{DMSO-d}_6$ )  $\delta_{\text{C}}$  (ppm): 162.43, 160.98, 159.21, 158.81, 154.11, 150.93, 146.62, 134.97, 131.96, 131.91, 127.59, 127.35, 126.42, 124.45, 120.92, 115.65, 115.41, 78.97, 66.12, 47.18, 44.07, 28.90, 28.85, 26.49, 13.97. MS ( $m/z$ , %): 564.4 ( $\text{M}^+$ , 3.1), 346 (8.6), 302.1 (6.4), 267.2 (30.2), 253.2 (48.3), 238.3 (43.9), 154.1 (35.8), 82.2 (31.08), 68.1 (100). Elem. anal. calcd. for  $\text{C}_{27}\text{H}_{29}\text{FN}_6\text{O}_3$  (504.5); C, 64.27; H, 5.79; N, 16.66. Found: C, 64.31; H, 5.72; N, 16.65.

**2.1.4.8 6-(4-(Aminomethyl) piperidin-1-yl)-1-((3-(3-chloro-4-fluoro phenyl)-4-oxo-3,4-dihydro quinazolin-2-yl) methyl)-3-methyl pyrimidine-2,4(1H,3H)-dione (9h).** White powder; yield 73%; m.p. 175–176 °C; IR (KBr,  $\text{cm}^{-1}$ ): 3442 ( $\text{NH}_2$ ), 3377 ( $\text{NH}_2$ ), 3063–3003 (CH), 2927–2853 (CH), 1699 (C=O), 1665 (C=O), 1607 (C=O), 1549 (C=N), 1497 (C=C), 1384 (C-N), 1241–1185 (C-O), 1110 (C-F), 780 (C-Cl).  $^1\text{H}$  NMR (300 MHz,  $\text{DMSO-d}_6$ )  $\delta_{\text{H}}$  (ppm): 8.16 (d, 1H,  $J = 7.2$  Hz, H-5-quinazolinone), 7.874–7.942 (m, 2H, aromatic), 7.745 (d, 1H,  $J = 8.1$  Hz, aromatic), 7.582–7.648 (m, 3H, aromatic), 5.127–5.262 (m, 2H, quinazolinone- $\text{CH}_2$ ), 5.052 (s, 1H, uracil), 4.015 (d, 2H,  $J = 11.7$  Hz,  $\text{NH}_2$ ), 3.124 (s, 3H,  $\text{CH}_3$ -uracil), 2.662 (t, 2H,  $J = 12.3$  Hz, aliphatic), 2.354 (d, 2H,  $J = 6.3$  Hz, piperidine- $\text{CH}_2$ - $\text{NH}_2$ ), 1.565–1.679 (m, 2H, aliphatic), 1.378–1.436 (m, 1H, aliphatic), 1.243–1.298 (m, 2H, aliphatic), 0.812–0.876 (m, 2H, aliphatic).  $^{13}\text{C}$  NMR (75 MHz,  $\text{DMSO-d}_6$ )  $\delta_{\text{C}}$  (ppm): 162.42, 161.08, 158.82, 158.69, 156.22, 154.05, 150.63, 146.59, 135.04, 132.84, 132.81, 131.15, 127.40, 126.42, 120.91, 117.64, 117.42, 79.09, 66.32, 47.31, 44.19, 38.81, 30.94, 28.93. MS ( $m/z$ , %): 524.3 ( $\text{M}^+$ , 1.95), 493.3 (2.26), 414.2 (2.67), 322.1 (5.05), 303.1 (11.37), 273.1 (73), 237.2 (100), 184 (27.09), 129 (46.08), 68.1 (77.48). Elem. anal. calcd. for  $\text{C}_{26}\text{H}_{26}\text{ClFN}_6\text{O}_3$  (524.98); C, 59.49; H, 4.99; N, 16.01. Found: C, 59.46; H, 4.52; N, 15.98.

**2.1.4.9 6-(4-(Amino methyl) piperidin-1-yl)-1-((3-(5-chloro-2-methoxy phenyl)-4-oxo-3,4-dihydro quinazolin-2-yl) methyl)-3-methyl pyrimidine-2,4(1H,3H)-dione (9i).** White-cream powder; yield 89%; m.p. 95–100 °C; IR (KBr,  $\text{cm}^{-1}$ ): 3433 ( $\text{NH}_2$ ), 3386 ( $\text{NH}_2$ ), 3064–3006 (CH), 2924–2850 (CH), 1692 (C=O), 1664 (C=O), 1608 (C=O), 1547 (C=N), 1473 (C=C), 1281 (C-N), 1249–1184 (C-O), 779 (C-Cl).  $^1\text{H}$  NMR (400 MHz,  $\text{DMSO-d}_6$ )  $\delta_{\text{H}}$  (ppm): 8.145 (d, 1H,  $J = 6.8$  Hz, H-5-quinazolinone), 7.91 (t, 1H,  $J = 7.6$  Hz, aromatic), 7.715 (d, 1H,  $J = 8$  Hz, aromatic), 7.680 (s, 1H, aromatic), 7.610 (t, 1H,  $J = 7.6$  Hz, aromatic), 7.555 (d, 1H,  $J = 7.2$  Hz, aromatic), 7.262 (d, 1H,  $J = 8.8$  Hz, aromatic), 5.099–5.227 (m, 2H, quinazolinone- $\text{CH}_2$ ), 5.073 (s, 1H, uracil),

4.021 (d, 2H,  $J = 1.6$  Hz,  $\text{NH}_2$ ), 3.71 (s, 3H,  $\text{CH}_3$ -uracil), 3.091 (s, 3H,  $\text{CH}_3$ -aromatic), 2.668 (t, 2H,  $J = 12$  Hz, aliphatic), 2.403 (d, 2H,  $J = 5.2$  Hz, piperidine- $\text{CH}_2$ - $\text{NH}_2$ ), 1.533–1.669 (m, 3H, aliphatic), 1.175–1.275 (m, 2H, aliphatic), 0.818–0.953 (m, 2H, aliphatic).  $^{13}\text{C}$  NMR (100 MHz,  $\text{DMSO-d}_6$ )  $\delta_{\text{C}}$  (ppm): 162.47, 160.35, 158.97, 154.24, 153.61, 151.01, 146.63, 135.10, 130.74, 129.52, 127.65, 127.35, 126.45, 124.97, 124.14, 120.68, 113.86, 79.22, 66.09, 56.21, 46.27, 44.06, 37.46, 28.72, 26.42. MS ( $m/z$ , %): 537.02 (M+, 1.6), 437.1 (1.5), 328.2 (3.6), 315.2 (20.3), 300.1 (27.5), 284.1 (30.3), 271.1 (46.07), 269.1 (100), 255.1 (23.5), 238.2 (14.8), 208.2 (9.5), 154.1 (16.8), 102.1 (19.7), 76.1 (45.5). Elem. anal. calcd. for  $\text{C}_{27}\text{H}_{29}\text{ClN}_6\text{O}_4$  (537.02); C, 60.39; H, 5.44; N, 15.65. Found: C, 60.42; H, 5.41; N, 15.63.

**2.1.5. General procedure for the synthesis of substituted 1-benzyl-6-chloro-3-methyl pyrimidine-2,4(1H,3H)-dione (11a–11c).** To a stirred solution of different benzyl bromides (**10a–10c**) (1 mmol) in THF (10 mL), 3-methyl-6-chlorouracil (**6**) (0.46 mmol) and DIPEA (0.5 mmol) were added at room temperature and left to stir for 6 hours at 40 °C and then cooled to room temperature. Water (10 mL) was added and the reaction mixture was stirred for 2 hours. The solids were filtered, washed with isopropanol (3 × 40 mL), and dried at 60 °C to afford the products (**11a–11c**).

**2.1.6. General procedure for the synthesis of 6-(4-(aminomethyl) piperidine-1-yl)-substituted-1-benzyl-3-methyl pyrimidine-2,4(1H,3H)-dione (12a–12c).** The same as step d in series a (**9a–9i**).

**6-(4-(Aminomethyl) piperidin-1-yl)-1-benzyl-3-methyl pyrimidine-2,4(1H,3H)-dione (12a).** Yellow powder; yield 75%; m.p. 107 °C; IR (KBr,  $\text{cm}^{-1}$ ): 3363 ( $\text{NH}_2$ ), 3343 ( $\text{NH}_2$ ), 3028–2935 (CH), 2911–2824 (CH), 1706 (C=O), 1648 (C=O), 1601 (C=N), 1451 (C=C), 1345–1311 (C–N),  $^1\text{H}$  NMR (300 MHz,  $\text{DMSO-d}_6$ )  $\delta_{\text{H}}$  (ppm): 7.305 (d, 2H,  $J = 6$  Hz, aromatic), 7.194–7.257 (m, 3H,  $J = 10$  Hz, aromatic), 5.293 (s, 1H, uracil), 4.971 (s, 2H, uracil- $\text{CH}_2$ ), 3.111 (s, 5H,  $\text{CH}_3$ -uracil,  $\text{NH}_2$ ), 2.823 (s, 1H, aliphatic), 2.507–2.567 (m, 2H, aliphatic), 2.438–2.449 (m, 2H, piperidine- $\text{CH}_2$ - $\text{NH}_2$ ), 1.665–1.704 (m, 2H, aliphatic), 1.362–1.448 (m, 1H, aliphatic), 1.123–1.158 (m, 3H, aliphatic),  $^{13}\text{C}$  NMR (75 MHz,  $\text{DMSO-d}_6$ )  $\delta_{\text{C}}$  (ppm): 162.66, 160.72, 152.71, 137.99, 128.99, 127.53, 126.95, 89.005, 51.34, 47.92, 47.29, 38.31, 29.39, 27.80. MS ( $m/z$ , %): 328.2 (M+, 15), 237.1 (31), 220.1 (22), 194.1 (14), 163.1 (16), 113.1 (17), 91 (100). Elem. anal. calcd. for  $\text{C}_{18}\text{H}_{24}\text{N}_4\text{O}_2$  (328.4); C, 65.83; H, 7.37; N, 17.06. Found: C, 65.83; H, 7.37; N, 17.06.

**6-(4-(Aminomethyl) piperidin-1-yl)-3-methyl-1-(4-methyl benzyl) pyrimidine-2,4(1H,3H)-dione (12b).** Cream powder; yield 71%; m.p. 95–98 °C; IR (KBr,  $\text{cm}^{-1}$ ): 3363 ( $\text{NH}_2$ ), 3294 ( $\text{NH}_2$ ), 2926 (CH), 2854 (CH), 1704 (C=O), 1646 (C=O), 1515 (C=N), 1446 (C=C), 1377 (C–N),  $^1\text{H}$  NMR (400 MHz,  $\text{DMSO-d}_6$ )  $\delta_{\text{H}}$  (ppm): 7.109–7.129 (m, 2H, aromatic), 7.066–7.086 (m, 2H, aromatic), 5.278 (s, 2H, uracil- $\text{CH}_2$ ), 4.923 (s, 1H, uracil), 3.106–3.122 (m, 5H,  $\text{CH}_3$ -uracil,  $\text{NH}_2$ ), 2.571 (t, 2H,  $J = 10.8$  Hz, aliphatic), 2.463 (d, 2H,  $J = 6.4$  Hz, piperidine- $\text{CH}_2$ - $\text{NH}_2$ ), 2.257 (s, 3H,  $\text{CH}_3$ ), 1.708 (d, 2H,  $J = 11.6$  Hz, piperidine- $\text{CH}_2$ - $\text{NH}_2$ ), 1.374–1.410 (m, 1H, aliphatic), 1.123–1.252 (m, 4H, aliphatic),  $^{13}\text{C}$  NMR (100 MHz,  $\text{DMSO-d}_6$ )  $\delta_{\text{C}}$  (ppm): 162.16, 160.22, 152.19, 136.18,

134.43, 128.95, 128.84, 126.53, 126.29, 88.39, 50.82, 47.24, 46.63, 37.59, 28.91, 27.28, 20.62. MS ( $m/z$ , %): 342.2 (M+, 12), 237.1 (23), 220.1 (13), 194.1 (10), 163 (8), 113 (11), 105 (100), 96 (17), 79 (12). Elem. anal. calcd. for  $\text{C}_{19}\text{H}_{26}\text{N}_4\text{O}_2$  (342.44); C, 66.64; H, 7.65; N, 16.36. Found: C, 66.64; H, 7.65; N, 16.36.

**6-(4-(Aminomethyl) piperidin-1-yl)-1-(4-bromo benzyl)-3-methyl pyrimidine-2,4(1H,3H)-dione (12c).** White powder; yield 86%; m.p. 93–96 °C; IR (KBr,  $\text{cm}^{-1}$ ): 3423 ( $\text{NH}_2$ ), 3386 ( $\text{NH}_2$ ), 2920 (CH), 2849 (CH), 1699 (C=O), 1652 (C=O), 1542 (C=N), 1445 (C=C), 1377 (C–N), 680 (C–Br).  $^1\text{H}$  NMR (400 MHz,  $\text{DMSO-d}_6$ )  $\delta_{\text{H}}$  (ppm): 7.294 (d, 2H,  $J = 8$  Hz, aromatic), 6.948 (d, 2H,  $J = 8$  Hz, aromatic), 5.016–5.092 (m, 1H, uracil), 4.685–4.718 (m, 2H, uracil- $\text{CH}_2$ ), 2.891–2.853 (m, 5H,  $\text{CH}_3$ -uracil,  $\text{NH}_2$ ), 2.642–2.745 (m, 1H, aromatic), 2.171–2.384 (m, 4H, aliphatic), 1.485–1.514 (m, 1H, aliphatic), 1.286–1.397 (m, 1H, aliphatic), 0.947–1.170 (m, 3H, aliphatic), 0.635–0.755 (m, 1H, aliphatic),  $^{13}\text{C}$  NMR (100 MHz,  $\text{DMSO-d}_6$ )  $\delta_{\text{C}}$  (ppm): 162.13, 160.01, 152.17, 136.96, 131.29, 131.18, 128.81, 128.84, 120.08, 88.74, 50.68, 46.92, 45.62, 36.26, 28.73, 27.32. MS ( $m/z$ , %): 408.1 (M+, 12), 237.1 (75), 220.1 (42), 194.1 (34), 168.9 (100), 112.9 (28), 95.9 (73), 81.9 (53), 67.9 (26), 56 (28), 44.1 (39). Elem. anal. calcd. for  $\text{C}_{18}\text{H}_{23}\text{BrN}_4\text{O}_2$  (407.31); C, 53.08; H, 5.69; N, 13.76. Found: C, 53.08; H, 5.69; N, 13.76.

## 2.2. Docking procedure

The 3D X-ray crystal structure of the DPP-4 receptor (PDB code: 4a5s) was selected from the Protein Data Bank (<http://www.rcsb.org>) based on the similarity of its co-crystal ligand to our designed compounds. The structure of the synthesized compounds was generated, minimized, and converted to pdbqt format. For the preparation of the pdbqt format of the protein, we removed the cognate ligand and water molecules, added missing hydrogen atoms, and finally merged non-polar hydrogens according to their corresponding carbons. All preparation was performed using the AutoDock Tools package (1.5.6). The docking procedure was done in a grid box with a size of 30 × 30 × 30 and a center of  $x = 20.05$ ,  $y = 33.12$ ,  $z = 55.75$  using AutoDock Vina (1.1.2) using an in-house batch script (DOCKFACE).<sup>39,40</sup> The exhaustiveness was set to 100, and other docking parameters were set as default. The binding interactions of the docked compounds and the receptor were analyzed using PLIP (fully automated protein–ligand interaction profiler).

## 2.3. Molecular simulation

Gromacs v5.0.4 was utilized as a platform to carry out MD simulation, and VMD v1.8.7 was employed as a visualization tool. The protein structure file was downloaded from [www.rcsb.org](http://www.rcsb.org) (PDB ID: 4a5s). The topology file for the ligand was generated using the PRODRG server, and the force field GRO-MOS96 53a6 was used during the MD simulation. The dimensions of the simulation box were defined as (12 12 12), and solvent spc216 was added to the whole system. After that the system was neutralized, and the physiological concentration of NaCl (0.15 M) was added to the system.

The equilibration procedure contained 3 phases, including restraining the ligand (force 1000 in three dimensions), using the *NVT* ensemble for 100 ps (temperature coupling algorithm: *v*-rescale; modified Berendsen thermostat) and finally incorporating the *NPT* ensemble for 100 ps (pressure coupling algorithm: Berendsen).

Afterward, final MD for 100 ns was performed on each system (temperature coupling algorithm: *v*-rescale, and pressure coupling algorithm: Parrinello–Rahman). After that the trajectories of the simulations were loaded into VMD for further analyses and visualization of the binding mode.

#### 2.4. *In vitro* DPP-4 assay

The DPP-4 inhibitory activities of the designed compounds were measured using a MAK 203 kit (Sigma-Aldrich, Germany), which works based on cleaving the non-fluorescent substrate (H-Gly-Pro-AMC) to generate fluorescent product 7-amino-4-methyl coumarin (AMC). AMC can emit fluorescence with a wavelength of 460 nm at an excitation wavelength of 360 nm. According to the protocol, the assay was performed by mixing 25  $\mu$ L of 4 $\times$  compounds with various concentrations and 50  $\mu$ L of inhibition reaction mix (49  $\mu$ L of DPP4 assay buffer with 1  $\mu$ L of DPP4 enzyme) in each well. A blank control (a well without the enzyme) for all concentrations of compounds and an enzymatic control (without a compound but with the same volume) were also included. Then, the plate was incubated at 37  $^{\circ}$ C for 10 minutes. Afterward, 25  $\mu$ L of the enzymatic reaction mix containing 23  $\mu$ L DPP4 assay buffer and DPP4 substrate was added to each reaction well (tests, blank and enzymatic control). Assays were performed in 96-well black plates using a plate reader (POLARstar Omega) (Germany). The fluorescence (FLU,  $\lambda_{\text{ex}} = 360/\lambda_{\text{em}} = 460$  nm) was measured on a microplate reader in kinetic mode for 30 minutes at 37  $^{\circ}$ C. The slope between the two times  $T_1$  and  $T_2$  in the linear range of the fluorescence plot ( $\Delta$ FLU/minute) was then obtained. The slope of all tested compounds was subtracted from the relevant sample blank to get the corrected measurement. The following formula was used to measure the percentage of relative inhibition for each compound:

$$\% \text{ Relative Inhibition} = \frac{(\text{Slope EC} - \text{Slope SM})}{\text{Slope EC}} \times 100$$

Slope SM = Slope of sample inhibitor

Slope EC = Slope of enzyme control

The  $IC_{50}$  values, which show the concentration of the compound with a 50% inhibitory effect on the enzyme, were determined for all compounds using Curve Expert 1.4. software and Excel 2016.

#### 2.5. Kinetic study of DPP-4 inhibition

The kinetic mechanism of DPP-4 inhibition was determined by Elman's method in four different concentrations (100, 50, 10, and 1  $\mu$ M) of one of the most potent compounds, **9e**. A double reciprocal plot was drawn as  $1/[\text{velocity}]$  against  $1/[\text{substrate}]$  at different concentration ratios of the substrate (H-Gly-Pro-AMC)

to the DPP-4 enzyme. The plots were drawn using a weighted least-squares analysis that assumed the variance of velocity ( $v$ ) to be a constant percentage of  $v$  for the entire data set. The slopes of these Lineweaver–Burk plots were then drawn against the concentration of **9e** in the weighted analysis, and  $K_i$  was determined as the intercept on the negative  $X$ -axis. Data analysis was performed with GraphPad Prism 8.0 software (GraphPad Software Inc.).

#### 2.6. Statistical analysis

The data were expressed as the mean  $\pm$  SD for each analysis. GraphPad Prism software was used to perform one-way ANOVA statistical analyses, followed by Tukey's multiple comparison test.

#### 2.7. Biological assay

**2.7.1. Cell lines and cell culture.** Human colorectal carcinomas (HT-29 and SW1116), non-small cell lung carcinoma (A549), and normal lung cells (MRC-5) were purchased from the National Cell Bank of Iran (NCBI, Pasteur Institute, Tehran, Iran). HT-29 was cultured in DMEM high glucose (Bio Idea, Iran) in the presence of 2% L-glutamine (Gibco, USA). For SW1116 and A549, RPMI 1640 medium (Bio Idea, Iran), and for MRC-5, DMEM/Ham's F12 (Bio Idea, Iran) were used. All media were also supplemented with 10% fetal bovine serum (FBS; Gibco, USA) and 1% penicillin–streptomycin (Biosera, France) and kept at 37  $^{\circ}$ C in a humidified  $CO_2$  incubator.

The antiproliferative activity of all designed compounds (**9a–9i** and **12a–12c**) was determined by standard 3-(4,5-dimethylthiazol-yl)-2,5-diphenyl-tetrazolium bromide (MTT) assay according to reported protocols.<sup>41</sup> The cells were harvested from culture using trypsin/EDTA 0.5% solution (Gibco/USA) and then were seeded in 96-well microplates at a density of  $1 \times 10^4$  cells per well for the HT-29 and  $15 \times 10^4$  cells per well for the MRC-5 cell line and  $8 \times 10^3$  cells per well for the A549 and SW1116 cell lines in 100  $\mu$ L of complete culture medium. After 24 h, each cell line was treated with five different concentrations of the designed compounds, and cisplatin and sitagliptin as positive controls (5 to 500  $\mu$ M) in a triplicate manner. We tried to maintain the final DMSO concentration, the solvent, at less than 0.1% to avoid its cytotoxic effect. Three untreated wells were considered as negative controls. After 72 hours, the media were removed and replaced with 100  $\mu$ L fresh media containing 0.5 mg  $mL^{-1}$  MTT solution. They were incubated for 4 hours at 37  $^{\circ}$ C in the incubator to create formazan purple crystals. The media were then replaced with 150  $\mu$ L of DMSO and incubated at 37  $^{\circ}$ C in the dark for 10 minutes to dissolve the crystals. The absorbance of individual wells was read at 490 nm using a microplate ELISA reader. To estimate and analyze the data, Excel 2016 and Curve Expert 1.4. were used. A plot of the percentage inhibition *versus* concentration was delineated and  $IC_{50}$ , demonstrating the concentration with 50% growth inhibition, was obtained. The data were presented as the mean  $\pm$  SD for each analysis. Statistical analyses were performed by one-way ANOVA and Tukey's multiple comparison tests using Graph Pad Prism 8.0

software (GraphPad Software Inc.). Values were considered significant when  $P < 0.05$ .

**2.7.2. Surface and intracellular staining of DPP-4 (CD26).** For surface staining, the cells were harvested and aliquoted at a density of  $25 \times 10^4$  cells in each tube and incubated with PE-conjugated anti-CD26 (Biolegend, USA) for 30 minutes in the dark. The unstained tube was used as the negative control for each cell line. The cells were then washed twice and stained with 2  $\mu\text{L}$  of 7-AAD (BD Biosciences, USA) to distinguish viable from nonviable cells. For intracellular staining, the harvested cells were first fixed with 1% paraformaldehyde (Sigma-Aldrich, Germany), washed and then permeabilized with  $1 \times$  BD Perm/Wash buffer (BD Biosciences) for 1 hour at 4  $^\circ\text{C}$ . The permeabilized cells were then stained with PE-conjugated anti-CD26 (Biolegend) for 30 minutes. The cells were washed 2 times with  $1 \times$  BD Perm/Wash buffer, re-suspended in Phosphate Buffered Saline (PBS  $1 \times$ ) buffer, and studied immediately on a FACSCalibur flow cytometer (BD Biosciences). The data were analyzed with FlowJo software.

**2.7.3. Apoptosis analysis.** To describe the ability of compound **9e** and **12c** to induce apoptosis in the HT-29 cell line, a PE Annexin V apoptosis detection kit with 7-AAD (Biolegend) was used. According to a previous protocol,<sup>42,43</sup>  $100 \times 10^3$  cells per 500  $\mu\text{M}$  of complete culture medium were seeded in a 24-well culture plate. After 24 hours, three different concentrations of **9e** (6, 12, 24  $\mu\text{M}$ ) and **12c** (15, 30, 60  $\mu\text{M}$ ) were used to treat the cells for a period of 24 and 72 hours. An untreated sample was considered as a negative control. Then, the treated and non-treated cells were trypsinized and washed two times with cold PBS  $1 \times$ . The pellets were dissolved in 50  $\mu\text{L}$  binding buffer and transferred to polystyrene tubes (BD Biosciences, USA), stained with 2  $\mu\text{L}$  of PE-conjugated AV and 2  $\mu\text{L}$  of 7-AAD and incubated at room temperature for 15 minutes in the dark. Finally, 300  $\mu\text{L}$  binding buffer was added and the sample was directly studied using a four-color FACSCalibur flow cytometer (BD Biosciences). The data were analyzed with FlowJo software.

**2.7.4. Cell cycle analysis.**  $100 \times 10^3$  HT-29 cells per 500  $\mu\text{M}$  were seeded in a 24-well plate and treated with three different concentrations of **9e** (6, 12, 24  $\mu\text{M}$ ) and **12c** (15, 30, 60  $\mu\text{M}$ ) for 24 and 72 hours. Then the cells were harvested and washed with cold PBS  $1 \times$ , stabilized slowly in cold 70% ethanol, and incubated at 4  $^\circ\text{C}$  for 7 days. The fixed cells were washed twice in PBS  $1 \times$  and centrifuged at  $400 \times g$  at 4  $^\circ\text{C}$ . Afterward, the cells were resuspended with 50  $\mu\text{L}$  ribonuclease A ( $100 \mu\text{g mL}^{-1}$ ), Sigma-Aldrich, Germany) to remove RNA. Finally, 200  $\mu\text{L}$  propidium iodide (PI, 50  $\mu\text{g mL}^{-1}$  solution) (Sigma-Aldrich, Germany) was added to stain DNA. The cells were analyzed on a four-color FACSCalibur flow cytometer (BD Biosciences) with the appropriate settings. Finally, the data were analyzed with FlowJo software.

### 3. Results and discussion

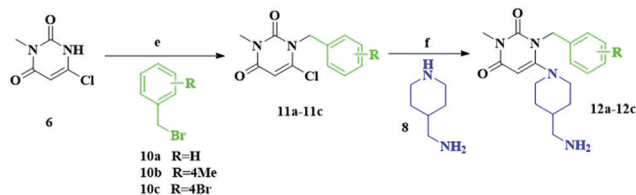
#### 3.1. Synthesis and Characterization of the amino-quinazolinone-pyrimidine hybrids (9a–9i)

The synthetic route for the preparation of the quinazolinone-pyrimidine hybrids (**9a–9i**) (series a) through four different

steps is displayed in Scheme 1. In the first step, anthranilic acid (**1**) was converted to benzoxazine-4-one (**3**) with chloroacetyl chloride (**2**) in the presence of a catalytic amount of diisopropyl ethyl amine (DIPEA) in dichloromethane (DCM) for 2 hours at room temperature. Next, a nucleophilic attack occurred between **3** and nine different substituted anilines (**4a–4i**) to give 2-(chloromethyl)-3-aromatic substituted quinazolinone-4(3*H*)-one derivatives **5a–5i** under acidic conditions at 60  $^\circ\text{C}$  with excellent yields (68–92%).<sup>44</sup> The third step of the reaction was done by replacing the chlorine atom at the side chain with 6-chloro-3-methyl-uracil (**6**) to achieve intermediates **7a–7i** using optimized conditions. For this purpose, different polar protic (EtOH and MeOH) and aprotic (DMF, MeCN, DCM, and THF) solvents were tested together with different temperatures, varied bases ( $\text{K}_2\text{CO}_3$ , NaH, DIPEA, and  $\text{Cs}_2\text{CO}_3$ ) and various time points. The optimized conditions were found to be in acetonitrile (MeCN) as a solvent under basic conditions of DIPEA and reflux for 24 hours. In the case of by-product creation, the compound was purified on a chromatography plate, using silica gel and 25% chloroform in *n*-hexane as an eluent. To achieve the final target compounds (**9a–9i**), 4-(aminomethyl) piperidine (**8**) was reacted with intermediates **7a–7i** through nucleophilic substitution under a moderate basic catalyst ( $\text{K}_2\text{CO}_3$ ) and iso-propyl alcohol as a solvent in high yields (69–89%). The chemical structures of all compounds were confirmed by IR,  $^1\text{H-NMR}$ ,  $^{13}\text{C-NMR}$ , and mass spectroscopies. In IR analysis, the stretching frequency of N–H bond in primary amine was observed at  $3363\text{--}3447 \text{ cm}^{-1}$  and  $3387\text{--}3294 \text{ cm}^{-1}$ . The significant feature of the  $^1\text{H NMR}$  spectrum of compounds **9a–9i** was a doublet peak at 3.605–4.021 ppm related to the  $\text{NH}_2$  proton. The two protons of  $\text{CH}_2$  which are between quinazolinone and the uracil ring appeared as a singlet for all compounds except **9b**, **9f**, **9h**, and **9i**. The peaks appearing as a doublet of doublets can be attributed to the existence of  $\text{CF}_3$ , 3,4-di-Me, 3Cl-4F, and 5Cl-2OMe groups on the phenyl ring, which can lead to nonequivalent protons in the compounds. The proton peak of uracil was indicated as a singlet at 4.813–5.33 ppm for all compounds except **9f**. The important piece of the  $^{13}\text{C NMR}$  spectrum of the compounds was a singlet peak related to C5 of the uracil scaffold, which appeared in the range of 78.97–88.74 ppm depending on the other substitutions. The carbon of the carbonyl group in the quinazolinone ring was displayed in the range of 162.15–162.99 ppm.

#### 3.2. Synthesis and Characterization of the amino-benzyl-pyrimidine hybrids (12a–12c)

The benzyl-pyrimidine hybrids (**12a–12c**) (series b) were prepared by known literature methods.<sup>44,45</sup> Firstly, 6-chloro-3-methyl-uracil (**6**) was reacted with three substituted benzyl bromides (**10a–10c**) in THF using DIPEA to achieve intermediates **11a–11c**. Then, 4-(aminomethyl) piperidine (**8**) was reacted with **11a–11c** under the optimized conditions described for step 3 in series a to get the final compounds (Scheme 2). The chemical structures of all compounds were confirmed by IR,  $^1\text{H-NMR}$ ,  $^{13}\text{C-NMR}$ , and mass spectroscopies. In IR analysis, the



**Scheme 2** Synthesis of the amino-benzyl-pyrimidine hybrids (**12a–12c**). Reagents and conditions: (e) DIPEA, THF, 40 °C, 6 h. (f) 4-(Aminomethyl) piperidine, *i*-PrOH, NaHCO<sub>3</sub>, MeCN, 65 °C, 24 h.

stretch bond of the primary amine was observed at 3363–3423 cm<sup>-1</sup> and 3386–3294 cm<sup>-1</sup>. The two protons of CH<sub>2</sub> which are between aryl and the uracil ring appeared as a singlet in the range of 4.72–4.97 ppm. The proton peak of position 5 in uracil appeared as a singlet except in the case of **12c**. The significant features of the <sup>13</sup>C NMR spectrum were a singlet peak related to C5 of the uracil scaffold, which appeared in the range of 88.39–89.00 ppm, and the peak of the carbonyl group at the uracil moiety, observed in the range of 162.13–162.65 ppm.

### 3.3. Molecular docking study

Molecular docking was performed to delve into the interactions, free binding energy, and molecular binding mode of the synthesized compounds against the DPP-4 enzyme. The range of free binding energy values was observed between -7.5 (**10b**) and -9.3 (**6e**), as displayed in Table 2. The binding mode of **9a**, **9e**, **12c**, and sitagliptin in the active site of the DPP-4 enzyme is provided in Fig. 2. As depicted in Fig. 2, the phenyl ring of the quinazolinone moiety in compound **9a** binds to the S<sub>2</sub>' subsite<sup>46</sup> *via* pi-pi interactions with Trp 629. Also, N-1 of the quinazolinone ring interacts through a hydrogen bond with Ser 630, and some hydrophobic interactions with the residues Tyr 547, Lys 554, and Tyr 631 were observed. The binding mode for

compound **9e** can be summarized by pi-pi interactions with Trp 629 located in the S<sub>2</sub>' site and the interaction of the carbonyl group at the C-4 position of the quinazolinone ring with Ser 630 of the catalytic triad in the S<sub>2</sub> pocket. The 4-phenoxy substituent occupying the S<sub>1</sub> subsite is aligned with the residues Tyr 662, Tyr 666, and Tyr 631 and might take a role in its enhanced DPP-4 activity compared to the other synthesized compounds. There are also hydrogen bond and pi-cation interactions through the carbonyl group and the N-3 position of uracil with Lys 554.

In compound **12c**, the 4-(aminomethyl) piperidine group formed salt bridges with Glu 206 and the 4-bromobenzyl group filled the S<sub>1</sub> pocket of the enzyme with Tyr 666 and Tyr 662. Furthermore, the carbonyl group at position 3 of uracil formed hydrogen bond interactions with Ser 630 of the catalytic triad and Arg 125 in the S<sub>2</sub> pocket. To explain the binding mode of sitagliptin, in brief, it should be announced that the three fluorophenyl moieties of sitagliptin were occupying the S<sub>1</sub> pocket *via* Tyr 662 and Tyr 666. In addition, a hydrogen bond between the NH group and His 740, Arg 125, and Ser 630 was observed (Fig. 2).

Several methods were introduced to verify the accuracy of the docking results,<sup>47,48</sup> including a re-docking simulation of the co-crystal ligand (N7F) in the active site of DPP4, which revealed a root mean square deviation (RMSD) of 0.4 Å. Meanwhile, the receiver operating characteristic (ROC) and enrichment factor (EF<sub>max</sub>)<sup>49</sup> were also studied. Firstly, a benchmark set of compounds with assay data against DPP-4 was retrieved from the ChEMBL database in the SMILES format.<sup>50</sup> The compounds were then converted to 3D mol<sup>2</sup> by DOCK-FACE, in-house batch script software. The ligands were classified according to their experimental data (IC<sub>50</sub>) as active and inactive (decoy). The resulting ligands were subjected to docking simulations as described for the co-crystal ligand. Finally, the binding energy of the best pose for each ligand was used to calculate the two metrics of the area under the curve of the ROC (AUC-ROC) curves and the enrichment factor (EF<sub>max</sub>).

The plots and results of ROC and EF<sub>max</sub> are shown in Fig. 3. The AUC-ROC of 0.922 and EF<sub>max</sub> of 3.2 verified that the docking scores could distinguish between active and inactive structures.

### 3.4. A molecular dynamics simulation study

Molecular dynamics simulations (MD) for the **9e** and **9f** compounds were performed to cover the space of moderate and high affinities against the DPP-4 enzyme. The protein-ligand complexes and individual root mean square deviations (RMSDs) of compounds **9e** and **9f** were achieved after 100 ns MD simulation, as seen in Fig. 4a. The plateau at the terminal part of the curves for the two compounds showed that the system is in the equilibrated state and has stability during the simulation.

According to Fig. 4b (the plot of the RMSD), a more stable pattern was observed for compound **9e** concerning **9f**. The energy values for ligands **9e** and **9f** at different time levels during the 100 ns simulation are displayed in Table 1. The van

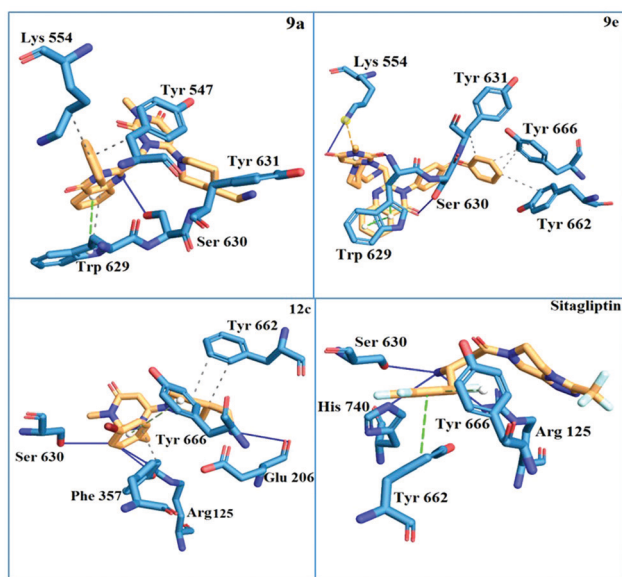


**Fig. 2** Interactions of **9a**, **9e**, **12c** and sitagliptin with the residues in the binding site of the DPP-4 receptor (4a5s).

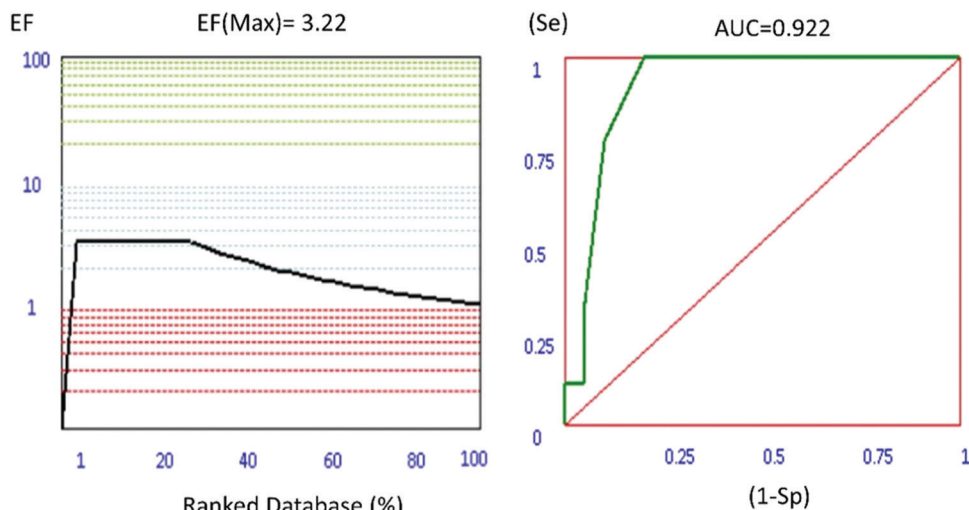


Fig. 3 Enrichment factor (left) and ROC (right) diagrams for the DPP-4 (4a5s) receptor.

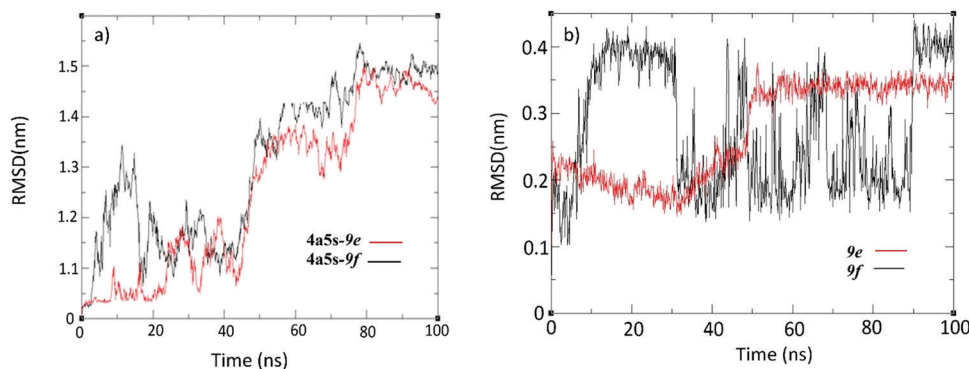


Fig. 4 (a) Root mean square deviation (RMSD) values of 4a5s-**9e** and 4a5s-**9f** as red and black, respectively, at different time levels during molecular dynamics (MD) simulation studies, and (b) RMSD values of the **9e** (red) and **9f** (black) ligands.

Table 1 Different types of intramolecular forces of the **9e** and **9f** complexes through MD simulation

Entry	van der Waals energy (kJ mol <sup>-1</sup> )	Electrostatic energy (kJ mol <sup>-1</sup> )	Polar solvation energy (kJ mol <sup>-1</sup> )	SASA energy (kJ mol <sup>-1</sup> )	Binding energy (kJ mol <sup>-1</sup> )
<b>9e</b>	-167.690	-74.239	125.773	-26.715	-132.872
<b>9f</b>	-115.754	-35.990	75.484	-12.604	-88.864

der Waals energy for compounds **9e** and **9f** was -167.690 and -115.754, respectively. This difference in energy levels indicates a more specific molecular shape for **9e** in comparison with **9f**. The same pattern can be observed while comparing other components of intramolecular forces in **9e** compared to **9f**. This result is suggestive of the more stable complex of **9e** in the active site of the enzyme.

According to the fluctuations of the amino acids displayed in the RMSF plot (Fig. 5), the domains covering residues 200–210, 550–700 and 910–920 were found to be the parts of the active site with the highest fluctuation during the simulation (Fig. 5b). In summary, both protein–ligand complexes have been stabilized under *NPT* conditions; however, **9e** has a more favorable effect on the DPP-4 enzyme.

### 3.5. Determination of DPP-4 inhibition and structure–activity relationship studies

The DPP-4 enzymatic activity of the synthesized compounds (**9a–9i** and **12a–12c**) was assayed by cleavage of H-Gly-Pro-amino methyl coumarin (H-Gly-Pro-AMC) as a fluorogenic substrate. The percentages of DPP-4 enzyme inhibition at concentrations of 100  $\mu$ M and IC<sub>50</sub> for each compound and sitagliptin (as a standard drug) are presented in Table 2. Generally, six derivatives (**9c**, **9d**, **9e**, **9g**, **12a**, and **12c**) had more than 50% inhibition at 100  $\mu$ M. **9e** with an IC<sub>50</sub> value of  $34.3 \pm 3.3$   $\mu$ M was found to be the most active hit compound. The structure–activity relationship for compounds **9a–9i** indicated that substitution of 4-phenoxy on ring A significantly increased the DPP-4 inhibitory activity. One possible reason for

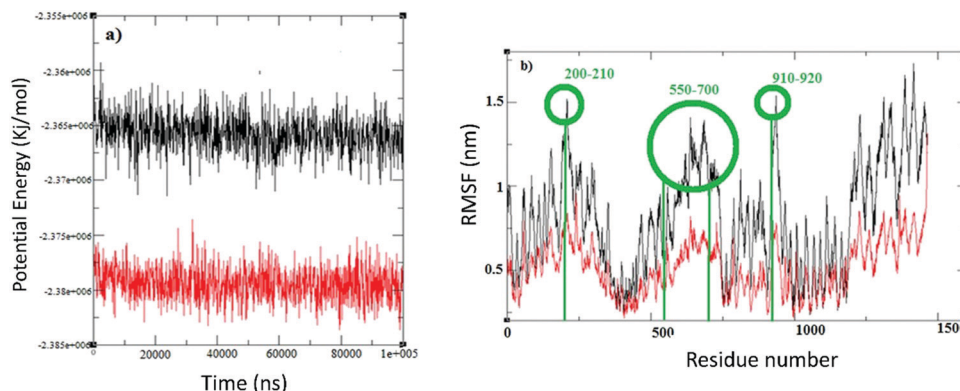


Fig. 5 (a) Potential energies of **6e**-4a5s and **6f**-4a5s interactions during  $10^{-5}$  ps MD simulation. (b) The root mean square fluctuation (RMSF) of the **9e** and **9f** complexes.

this observation could be the better accommodation of the 4-phenoxy phenyl ring despite its greater surface area into the  $S_1$  pocket of the enzyme. This result is also in accord with the binding energies obtained from docking experiments. In addition, having a higher hydrophilicity/lipophilicity balance of **9e** might increase its solubility ( $\log P = 3.4$ ) and so its penetration into the target cells. Among those compounds containing mono-substituted groups (**9b**, **9c**, and **9d**), compounds **9c** and **9d** with electron-withdrawing groups at position 4 of ring A showed higher DPP-4 inhibitory activities compared to **9b** bearing  $\text{CF}_3$  at position 3 (in the order of  $\text{F} > \text{Cl}$ ). The results also showed that removing the substitution on ring A in **9a** even led to a greater decrease in the inhibitory activity. In the case of the disubstituted compounds (**9f**, **9g**, and **9h**), compound **9g**, which has an electron-withdrawing

and an electron-releasing group at position 3 and 4 of ring A, respectively, showed higher DPP-4 inhibitory activity than the others. On the other hand, the **9i** derivative tethering a 5-chloro-2-methoxy group displayed lower inhibitory activities than the other compounds. The results collectively indicated that the mono-substituted compounds showed higher DPP-4 inhibitory activities than the disubstituted derivatives. In addition, the combination of electron-withdrawing and releasing groups influenced the DPP-4 inhibitory activity of the compounds. Moreover, the quinazoline-pyrimidine hybrid with a bulky substituent *i.e.*, **9e**, had higher activity, probably due to complete accommodation into the  $S_1$  pocket of the enzyme.

A comparison between the amino-benzyl-pyrimidine hybrids (**12a**-**12c**) also indicated that **12a** with no substituent on ring A

Table 2 DPP-4 inhibitory activity, binding energy ( $\text{kcal mol}^{-1}$ ) and  $\log P$  of the synthesized compounds

Entry	R	%DPP-4 Enzyme inhibition at $100 \mu\text{M}^a$	$\text{IC}_{50}$ ( $\mu\text{M}$ )	$\log P$	Binding energy ( $\text{kcal mol}^{-1}$ )
<b>9a</b>	H	$27.1 \pm 0.67$	$249.0 \pm 9$	1.9	-8.8
<b>9b</b>	3- $\text{CF}_3$	$23.6 \pm 6.2$	$197.0 \pm 11$	2.8	-8.9
<b>9c</b>	4-F	$62.1 \pm 1.0$	$62.6 \pm 2.1$	2.0	-8.2
<b>9d</b>	4-Cl	$53.5 \pm 1.1$	$87.7 \pm 2.7$	2.4	-8.7
<b>9e</b>	4-Phenoxy	$78.3 \pm 1.7$	$34.3 \pm 3.3$	3.4	-9.3
<b>9f</b>	3,4-diMe	$30.5 \pm 8.2$	$157.0 \pm 4.5$	2.8	-8.1
<b>9g</b>	3F-4Me	$50.9 \pm 0.84$	$100.1 \pm 0.3$	2.5	-8.6
<b>9h</b>	3Cl-4F	$31.5 \pm 0.95$	$195.0 \pm 5$	2.6	-8.5
<b>9i</b>	5Cl-2OMe	$30.8 \pm 6.5$	$210.0 \pm 1.2$	2.3	-8.8
<b>12a</b>	H	$63.8 \pm 3.8$	$85.0 \pm 2.6$	1.1	-8.5
<b>12b</b>	4-Me	$25.8 \pm 1.3$	$281.0 \pm 0.5$	1.6	-7.5
<b>12c</b>	4-Br	$51.5 \pm 1.3$	$98.3 \pm 1.2$	2.0	-8.6
Sitagliptin	—	$0.1 \mu\text{M}$	$1 \mu\text{M}$	2.2	-9.3
		$67.0 \pm 1.4$	$91.0 \pm 2.8$		

<sup>a</sup> Values represent mean  $\pm$  standard deviation SD of three independent experiments.

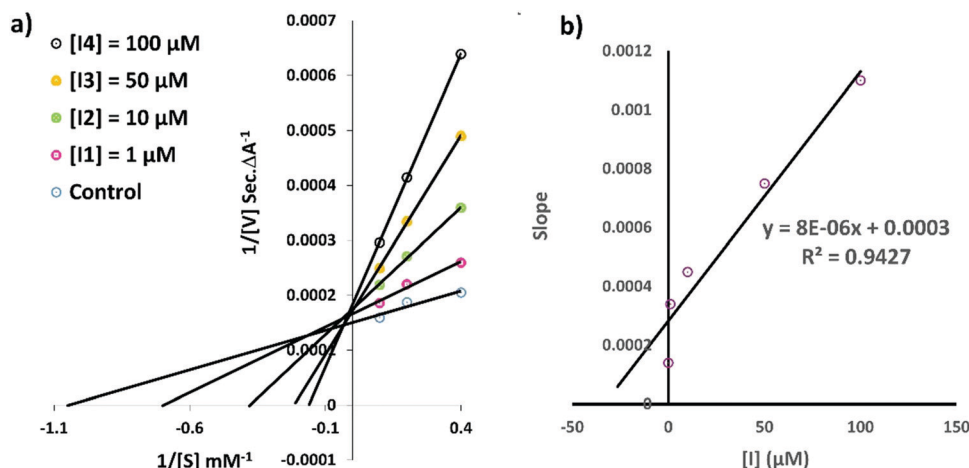


Fig. 6 Kinetics of DPP-4 inhibition of compound **9e**: (a) Lineweaver–Burk plot, and (b) Lineweaver–Burk secondary plot.

showed higher inhibitory activity against DPP-4 than **12b** and **12c**, in the order of H > Br > Me.

### 3.6. Kinetic study of DPP-4 inhibition

The pharmacokinetic profile of **9e**, the most potent DPP-4 inhibitor compound, was determined by the analysis of the Lineweaver–Burk (double-reciprocal) plot. Plots of  $1/V$  versus  $1/[S]$  for DPP-4 inhibition displayed a competitive inhibitory mode by the same Y-intercept, and different slopes and X-intercept at increasing concentration of the inhibitor, 0, 1, 10, 50 and 100  $\mu\text{M}$  (Fig. 6a). The  $K_i$  value (inhibition constant value) was found to be 33.24  $\mu\text{M}$  for **9e** as the most potent compound using the Michaelis–Menten equation (Fig. 6b).

### 3.7. In silico Physicochemical parameter (ADME) prediction

The physicochemical properties of all synthesized compounds and sitagliptin were calculated using the tool at <http://www.swissadme.ch/>, and the results are revealed in Table 3.

The molecular weight ( $M_w$ ) of most compounds was in the range of 328–566. The  $\log P$  values displayed that all of the compounds have reasonable lipophilicity. The hydrogen bond properties (as donors or acceptors), total polar surface area (TPSA), and rotatable bond number of all designed compounds are within the acceptable limit. Generally, the data indicated that all of the compounds followed Lipinski's rule of five except the  $M_w$  in only some cases.

The drug-likeness and Absorbance Distribution Metabolism and Excretion (ADME) properties of all compounds and sitagliptin were derived from the preADMET online server (<http://preadmet.bmdrc.org/>). The ADME properties, including Human Intestinal Absorption (HIA), *in vitro* Caucasian colon adenocarcinoma cell permeability (Caco-2), skin permeability, *in vitro* Plasma Protein Binding (PPB) and *in vivo* Blood–Brain Barrier penetration (BBB) are shown in Table 4. HIA analysis indicated that all compounds displayed good human intestinal absorption (HIA), which causes quick absorption from the intestine to the bloodstream. The Caco-2 permeability parameters suggest that these

Table 3 Physicochemical properties of the synthesized compounds

Entry	$M_w^a$	$\log P^b$	HBD <sup>c</sup>	HBA <sup>d</sup>	TPSA (Å <sup>2</sup> ) <sup>e</sup>	n-RB <sup>f</sup>	Lipinski violation
<b>9a</b>	472.5	1.9	1	5	108.1	5	0
<b>9b</b>	540.5	2.8	1	8	108.1	6	1
<b>9c</b>	490.5	2.0	1	6	108.1	5	0
<b>9d</b>	507.0	2.4	1	5	108.1	5	1
<b>9e</b>	566.6	3.4	1	7	114.0	7	1
<b>9f</b>	500.1	2.8	1	5	108.1	5	1
<b>9g</b>	504.6	2.5	1	6	108.1	5	1
<b>9h</b>	524.9	2.6	1	6	108.1	5	1
<b>9i</b>	537.0	2.3	1	6	117.4	6	1
<b>12a</b>	328.4	1.1	1	3	73.3	4	0
<b>12b</b>	342.4	1.6	1	3	73.3	4	0
<b>12c</b>	407.3	2.0	1	3	73.3	4	0
Sitagliptin	407.3	2.2	1	10	77.0	6	0
Rule of Lipinski	$\leq 500$	$\leq 5$	$\leq 5$	$\leq 10$	$\leq 140$	$\leq 10$	$\leq 1$

<sup>a</sup> Molecular weight ( $M_w$ ). <sup>b</sup> Logarithm of the partition coefficient between *n*-octanol and water ( $\log P$ ). <sup>c</sup> Number of hydrogen bond donors (HBD). <sup>d</sup> Number of hydrogen bond acceptors (HBA). <sup>e</sup> Topological polar surface area (TPSA). <sup>f</sup> Number of rotatable bonds (nRB).

Table 4 *In silico* ADME of the synthesized compounds

Entry	Absorption		Distribution		
	% HIA <sup>a</sup>	<i>In vitro</i> caco-2 cell permeability (nm s <sup>-1</sup> )	<i>In vitro</i> skin permeability (log $K_p$ , cm h <sup>-1</sup> )	% <i>In vitro</i> plasma protein bonding	% BBB <sup>b</sup>
<b>9a</b>	98.14	20.87	-3.7	54.7	0.17
<b>9b</b>	97.95	21.5	-2.5	73.4	0.32
<b>9c</b>	98.12	21.64	-4.0	59.5	0.25
<b>9d</b>	97.46	22.7	-3.8	71.0	0.31
<b>9e</b>	97.65	24.43	-2.7	80.9	0.29
<b>9f</b>	98.24	21.55	-3.6	50.9	0.15
<b>9g</b>	97.97	21.18	-4.0	66.0	0.17
<b>9h</b>	97.45	22.55	-4.0	74.25	0.35
<b>9i</b>	97.99	23.03	-3.9	65.91	0.24
<b>12a</b>	97.19	21.16	-3.8	35.71	0.03
<b>12b</b>	97.19	21.14	-3.8	41.05	0.08
<b>12c</b>	96.73	24.31	-3.8	57.72	0.08
Sitagliptin	96.90	30.6	-2.86	64.09	0.02

<sup>a</sup> Human intestinal absorption. <sup>b</sup> *In vivo* blood–brain barrier penetration.

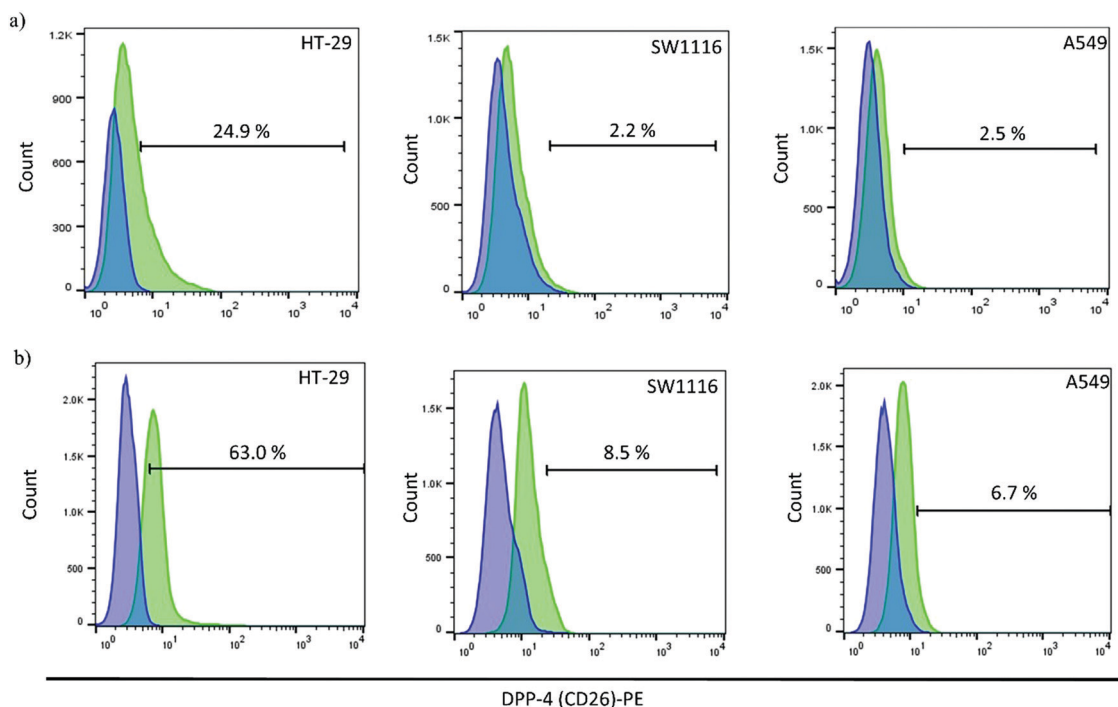


Fig. 7 Expression profile of DPP-4 (CD26)-PE in HT-29, SW1116 and A549. The stained diagrams (green) were overlaid on the corresponding unstained diagrams (blue) in both the surface (a) and intracellular (b) regions.

compounds have moderate permeability for penetration of biological membranes. Compounds **9b** and **9e** have useful skin penetration ( $K_p = -2.5$  and  $-2.76 \text{ cm h}^{-1}$ ) compared to sitagliptin ( $K_p = -2.86 \text{ cm h}^{-1}$ ). Also, most of the compounds bound moderately to plasma protein and so can diffuse or transport across the cell membranes. Moreover, the designed compounds showed low blood-brain barrier percentages and probably will not exert a considerable neurotoxic effect.

### 3.8. Flow cytometric analysis of DPP-4 (CD26) expression

DPP-4 (CD26) is a transmembrane glycoprotein expressed in different cell types, including tumor cells. It has been shown

that DPP-4 (CD26) expression is associated with immune regulation, which is mainly exerted through enzymatic cleavage of cytokines and interfering with T cell activation and cell migration.<sup>51,52</sup> In this study, to investigate the activity of the designed compounds as DPP-4 (CD26) inhibitors, we first determined the expression of the DPP-4 (CD26) marker in the investigated cells in both the surface and intracellular regions (Fig. 7). For surface-staining, harvested cells were also stained with 7-AAD vital dye to efficiently exclude nonspecific binding usually observed in nonviable cells; the frequency of DPP-4 (CD26) positive cells was then determined in 7-AAD neg viable cells. The maximum surface and intracellular expressions of

Table 5 *In vitro* cytotoxic activity of the novel designed compounds on the studied cancerous cell lines

Entry	R	$(IC_{50} \pm SD)^a \mu\text{M}$			
		HT-29	SW1116	A549	MRC-5
9a	H	88.6 ± 11.4	85.4 ± 5	229 ± 1	316 ± 6.8
9b	3-CF <sub>3</sub>	103.15 ± 3.1	163.2 ± 3.75	256.45 ± 4.95	292.5 ± 10.3
9c	4-F	48.4 ± 3	54.0 ± 1	192 ± 3	213.7 ± 4.5
9d	4-Cl	36.1 ± 2.1	58.3 ± 3.35	125.9 (±3.9)	143 ± 5.6
9e	4-Phenoxy	10.67 ± 0.3	19.03 ± 0.03	60.5 ± 2.7	85.2 ± 3.8
9f	3,4-diMe	69.15 ± 2.6	129.4 ± 2.5	243.5 ± 4.5	306 ± 10.8
9g	3F-4Me	62.1 ± 1.1	63.5 ± 0.5	168.25 ± 0.05	217.5 ± 5.1
9h	3Cl-4F	69.1 ± 2.4	70.4 ± 1.94	227.65 ± 1.35	324 ± 5.6
9i	5Cl-2OMe	67.9 ± 2.2	103 ± 7	182.25 ± 2.75	196 ± 2.3
12a	H	129.5 ± 11.5	160.7 ± 2.25	277.5 ± 14.5	417 ± 11.8
12b	4-Me	78.3 ± 7.3	190.9 ± 1.95	291.25 ± 7.25	359 ± 6.2
12c	4-Br	27.9 ± 6.5	49.2 ± 1.2	120.5 ± 16.5	142 ± 5.8
Sitagliptin	—	35 ± 1.2	389 ± 2.5	> 500	
Cisplatin	—	107.1 ± 2.3	41.69 ± 1.32	5.7 ± 1.6	13.5 ± 1.5

<sup>a</sup> Measured in two or three independent experiments.

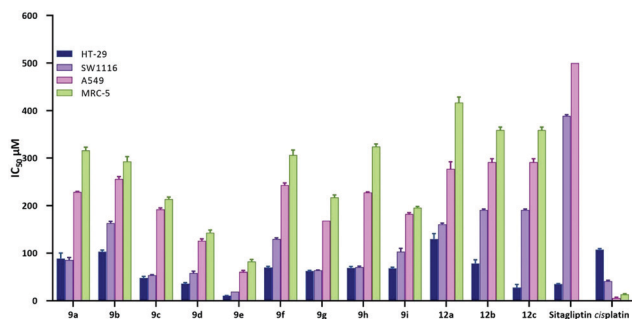


Fig. 8 Cytotoxic effects of compounds **9a–9i**, **12a–12c**, sitagliptin and cisplatin on HT-29, SW1116, and A549 carcinoma and MRC-5 normal lines.

DPP-4 (CD26) were observed in colorectal carcinoma cell lines HT-29 (24.9% and 63%) followed by SW1116 (2.22% and 8.48%), while the lung cancer cell line (A549) showed the

minimum percentage of both surface and intracellular DPP-4 (CD26) expression (2.59% and 6.72%). These observations partly explain the better cytotoxic activities of the designed compounds as DPP-4 inhibitors in the HT-29 cell line. Surface and intracellular expression of DPP-4 (CD26) were reported in other studies on cancer<sup>53,54</sup> as well as at <https://www.proteina.tlas.org/>.

### 3.9. Cytotoxic activity studies

The tumor growth inhibition of the designed compounds was evaluated against four human cell lines including A549 (non-small cell lung carcinoma), SW1116 (colon carcinoma), HT-29 (colorectal adenocarcinoma) and MRC-5 (normal cells isolated from human lung tissue). The results were compared to cisplatin and sitagliptin as the standard drugs. As summarized in Table 5, all compounds showed desirable inhibitory effects on both the colorectal and lung carcinoma cell lines compared to sitagliptin as

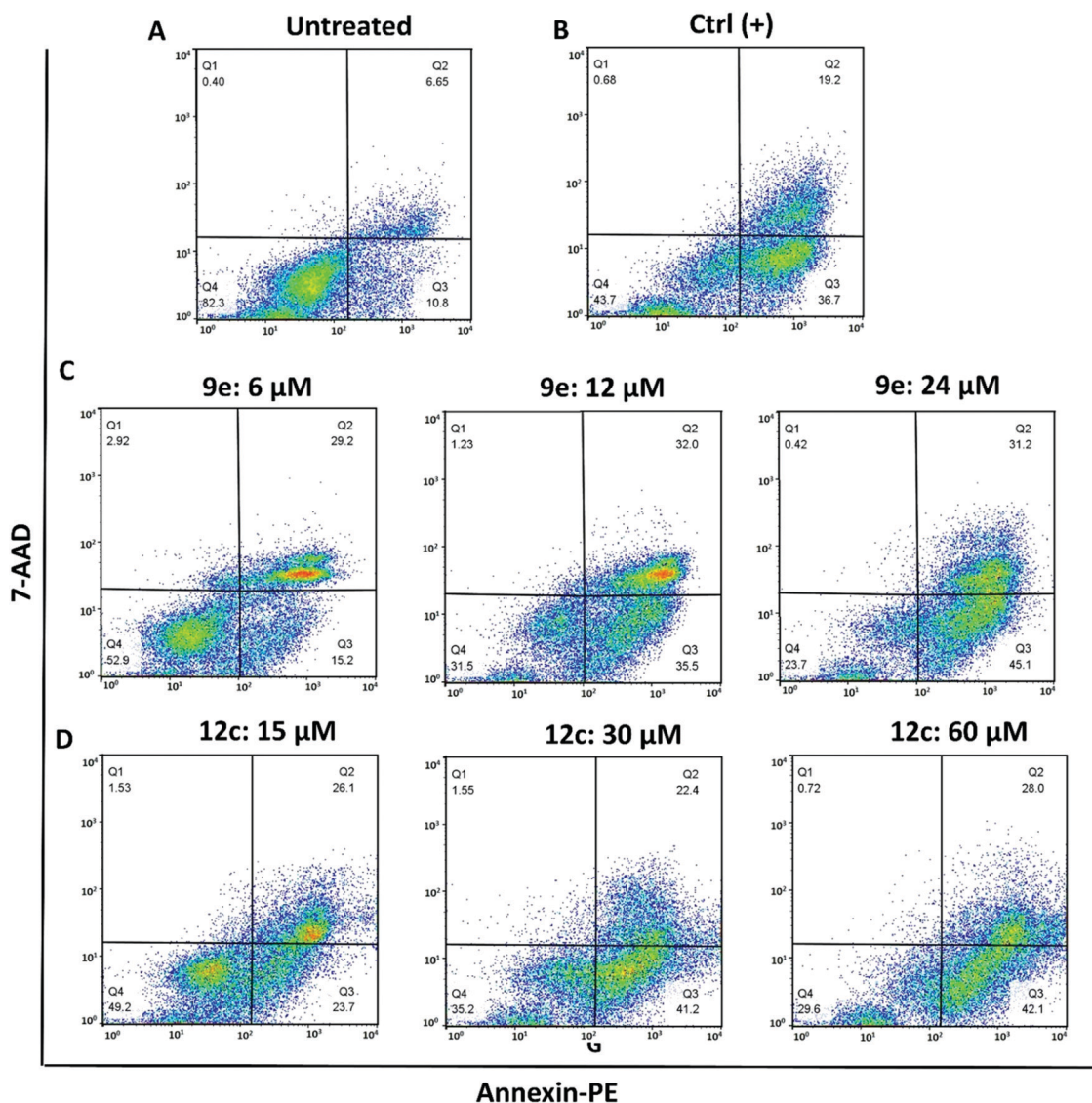


Fig. 9 Flow cytometric analysis of the apoptotic effect of **9e** and **12c**. HT-29 cells for 72 h with **9e** (C) and **12c** (D). Untreated cells (A) were mostly viable as they were negative for both Annexin V and 7-AAD. Ctrl (+) heated at 56 °C (B).

the standard drug. The best cytotoxic effect was observed on HT-29, followed by SW1116 and less on A549, probably related to higher expression of DPP-4 (CD26) in the HT-29 cell line than the others. All compounds also showed a lesser cytotoxic effect on the normal cells (MRC-5) in comparison to the carcinoma cell lines, which showed their relative selectivity between tumorigenic and non-tumorigenic cell lines. Almost all compounds (except **12a**) showed significantly higher cytotoxic activities than cisplatin and sitagliptin on the HT-29 cell line (Table S1, ESI<sup>†</sup>). Among the two series, compounds **9e** with an  $IC_{50}$  of  $10.67 \pm 0.3 \mu\text{M}$  and **12c** with an  $IC_{50}$  of  $27.9 \pm 6.5 \mu\text{M}$  were the most potent compounds compared to sitagliptin ( $IC_{50} = 35 \pm 1.2 \mu\text{M}$ ) and cisplatin ( $IC_{50} = 107.1 \pm 2.3 \mu\text{M}$ ), Fig. 8. Similarly, these two compounds ( $IC_{50} = 19.03 \pm 0.03 \mu\text{M}$  for **9e** and  $49.2 \pm 1.2$  for **12c**) showed the best inhibitory effects on SW1116, another colorectal cell line. Meanwhile, in the case of A549, all compounds presented significantly lower activities  $IC_{50}$  in the range of 60–291  $\mu\text{M}$  (Table 5 and Table S3, ESI<sup>†</sup>). The structure–activity relationship also indicated that in series **9a–9i**, among the mono-substituted groups, it seems that having bulky (4-phenoxy) and halogen groups in the order of  $\text{Cl} > \text{F} > \text{CF}_3$  on ring A increases the antiproliferative activity, which is compatible with the results obtained with the DPP-4 inhibitory assay. **9e** with the best DPP-4 inhibitory activity ( $IC_{50} = 34.3 \mu\text{M}$ ) also had higher cytotoxic activity.

On the other hand, the comparison among **9f**, **9g**, **9h**, and **9i** bearing disubstituted groups indicated that electronic balance between electron-withdrawing and releasing substituents improves the anti-tumor activity of the compound. In series **b** (**12a–12c**), it is clear that the presence of a halogen group (Br) at the para position of ring A significantly increases their anti-tumor activities. There was good agreement between the DPP-4 inhibitory activity and anticancer activity of this series.

### 3.10. Determining the apoptotic effect of **9e** and **12c** on the HT-29 cell line

Apoptosis was measured using an Annexin V (AV)-7-amino-actinomycin D (7-AAD) apoptosis detection kit by the flow cytometry method. This technique allows us to detect the viable cells ( $\text{AV}^{\text{neg}}/7\text{-AAD}^{\text{neg}}$ ), early phase apoptotic cells ( $\text{AV}^{\text{pos}}/7\text{-AAD}^{\text{neg}}$ ), late phase apoptotic cells ( $\text{AV}^{\text{pos}}/7\text{-AAD}^{\text{pos}}$ ), and necrotic cells ( $\text{AV}^{\text{neg}}/7\text{-AAD}^{\text{pos}}$ ). In this method, fluorochrome-labeled AV can especially detect phosphatidylserine that translocates to the outer membrane during apoptosis. 7-AAD is a DNA specific dye that distinguishes live and dead cells. The apoptotic effect of **9e** and **12c** on HT-29 cells was evaluated in three different concentrations (6, 12, and 24  $\mu\text{M}$  for **9e** and 15, 30, and 60  $\mu\text{M}$  for **12c**) after 24 and 72 hours. The results showed that during the first 24 hours, neither of the **9e** and **12c** compounds could induce apoptosis in the HT-29 cells

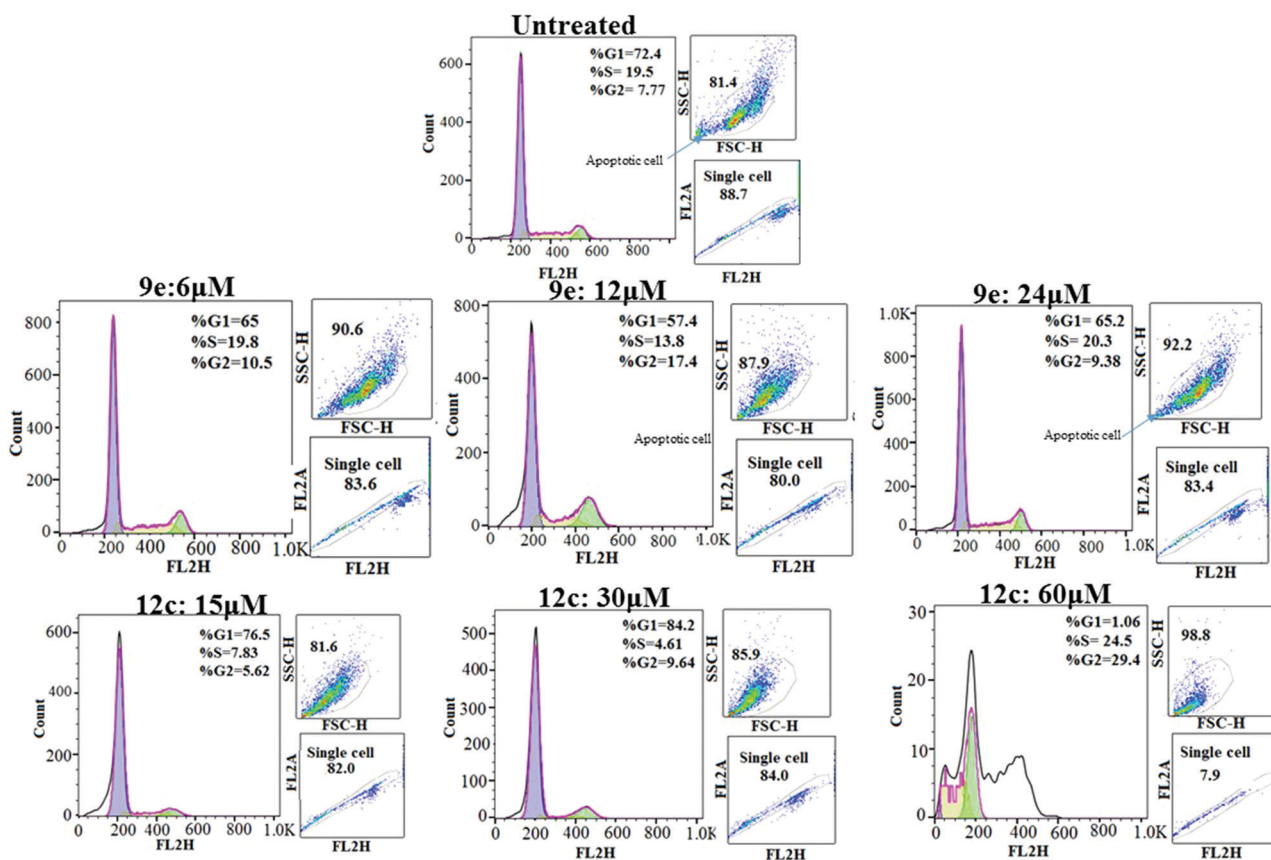


Fig. 10 The effect of **9e** and **12c** on the cell cycle in the HT-29 cell line after 72 hours of treatment.

(Fig. S58, ESI<sup>†</sup>), but the percentages of AV positive cells increased from 18% to 44%, 67% and 77% for **9e** and 50%, 64% and 70% for **12c** after 72 hours of treatment (Fig. 9). These results implied that the apoptotic effects of **9e** and **12c** in the HT-29 cell line are dose and time-dependent.

### 3.11. The potential effect of **9e** and **12c** on the HT-29 cells' cell cycle

A flow cytometry-based method was performed to investigate the cell cycle distribution of the most potent compounds of both series (**9e** and **12c**) on the HT-29 cell line. For this purpose, the HT-29 cells were treated with three different concentrations of **9e** (6  $\mu$ M, 12  $\mu$ M, and 24  $\mu$ M) and **12c** (15  $\mu$ M, 30  $\mu$ M, and 60  $\mu$ M) compared to untreated cells for 24 and 72 hours. The cell cycle profiles after 24 hours and 72 hours are depicted in Fig. 10 and Fig. S59 (ESI<sup>†</sup>), respectively. As could be seen, after 72 hours of incubation, the cells treated with 6  $\mu$ M and 12  $\mu$ M of **9e** showed accumulation in the G2/M phase compared with the untreated cells, 10.5% and 17.4% vs. 7.77%, respectively. Similar results were also observed for **12c** with 15  $\mu$ M (5.62%), 30  $\mu$ M (9.64%), and 60  $\mu$ M (29.4%) (Fig. 12, ESI<sup>†</sup>). The results indicated that compounds **9e** and **12c** could induce partial cell cycle arrest in G2/M phases.

## 4. Conclusion

In the present research, certain quinazolinone-pyrimidine and benzyl-pyrimidine hybrid derivatives were designed, synthesized, and evaluated for their DPP-4 inhibitory activity and antiproliferative potential. Our results illustrated that compound **9e**, containing a 4-phenoxy moiety on the phenyl ring at position 3 of the quinazolinone scaffold, was the most potent derivative with a DPP-4 inhibitory function and cytotoxic effect. Furthermore, inhibition kinetics analysis indicated that **9e** acted in a competitive inhibitory mode. The SAR studies reported that the substitution of a bulky substituent or an electron-withdrawing with an electron-donating group on the phenyl ring increased the DPP-4 inhibitory activity. The highest anticancer activity belonged to compound **9e**, particularly on colorectal cancer HT-29 and SW1116 cell lines. The greater cytotoxic activity of the studied compounds could be attributed to the greater expression of DPP-4 (CD26) in both the surface and intracellular compartments in the colorectal cancer cell lines in comparison with the lung cell lines as demonstrated with the flow cytometry method.

A good correlation was observed between the CD26 expression and the anticancer activity as well as the DPP-4 inhibitory effect for compounds **9e** and **12c** (as the most potent compounds in each series). Not only could these compounds induce apoptosis in the HT-29 cell line in a dose and time-dependent manner, but also they could arrest cells in the G2/M phase. The physicochemical and drug-likeness properties of the designed compounds indicated that the compounds are compatible with the Lipinski rule, and **9e** is a moderate and selective candidate as a DPP-4 inhibitor and also acted as

potent candidate in colon cancer treatment, yet they need further optimized modifications.

## Conflicts of interest

There are no conflicts to declare.

## Acknowledgements

Financial assistance from the Shiraz University of Medical Sciences by way of grant number 97-01-05-17869 is gratefully acknowledged.

## References

- 1 G. Ghersi, Q. Zhao, M. Salamone, Y. Yeh, S. Zucker and W.-T. Chen, *Cancer Res.*, 2006, **66**, 4652–4661.
- 2 M. Gonzalez-Gronow, H. E. Grenett, M. R. Weber, G. Gawdi and S. V. Pizzo, *Biochem. J.*, 2001, **355**, 397–407.
- 3 P. A. Havre, L. H. Dang, K. Ohnuma, S. Iwata, C. Morimoto and N. H. Dang, *BMC Cancer*, 2013, **13**, 517.
- 4 A. J. Scheen, *Expert Opin Drug Discovery*, 2015, **14**, 505–524.
- 5 S. H. Tella and M. S. Rendell, *Expert Opin Drug Discovery*, 2015, **14**, 127–140.
- 6 A. Beckenkamp, S. Davies, J. B. Willig and A. Buffon, *Tumor Biol.*, 2016, **37**, 7059–7073.
- 7 P. A. Havre, M. Abe, Y. Urasaki, K. Ohnuma, C. Morimoto and N. H. Dang, *Front. Biosci.*, 2008, **13**, 1634–1645.
- 8 B. Pro and N. H. Dang, *Histol. Histopathol.*, 2004, **4**, 1345–1351.
- 9 R. Bishnoi, Y. R. Hong, C. Shah, A. Ali, W. P. Skelton IV and J. Huo, *et al.*, *Cancer Med.*, 2019, **8**, 3918–3927.
- 10 S. Nishina, A. Yamauchi, T. Kawaguchi, K. Kaku, M. Goto and K. Sasaki, *et al.*, *Cell Mol. Gastroenterol Hepatol.*, 2019, **7**, 115–134.
- 11 C. Hollande, J. Boussier, J. Ziai, T. Nozawa, V. Bondet and W. Phung, *et al.*, *Nat. Immunol.*, 2019, **20**, 257–264.
- 12 M. Kraman, P. J. Bambrough, J. N. Arnold, E. W. Roberts, L. Magiera and J. O. Jones, *et al.*, *Science*, 2010, **330**, 827–830.
- 13 K. Ohnuma, R. Hatano and C. Morimoto, *Nat. Immunol.*, 2015, **16**, 791–792.
- 14 T. Iino, Y. Sasaki, M. Bamba, M. Mitsuya, A. Ohno and K. Kamata, *et al.*, *Bioorg. Med. Chem. Lett.*, 2009, **19**, 5531–5538.
- 15 K. Lin, Z. Cai, F. Wang, W. Zhang and W. Zhou, *Chem. Pharm. Bull.*, 2013, **c12**-01046.
- 16 A. Padmaja, C. Rajasekhar, A. Muralikrishna and V. Padmavathi, *Eur. J. Med. Chem.*, 2011, **46**, 5034–5038.
- 17 H. Xie, L. Zeng, S. Zeng, X. Lu, X. Zhao and G. Zhang, *et al.*, *Eur. J. Med. Chem.*, 2013, **68**, 312–320.
- 18 P. M. Chandrika, T. Yakaiah, A. R. R. Rao, B. Narsaiah, N. C. Reddy and V. Sridhar, *et al.*, *Eur. J. Med. Chem.*, 2008, **43**, 846–852.

- 19 M. Dupuy, F. Pinguet, O. Chavignon, J.-M. Chezal, J.-C. Teulade and J.-P. Chapat, *et al.*, *Chem. Pharm. Bull.*, 2001, **49**, 1061–1065.
- 20 Y. Takase, T. Saeki, N. Watanabe, H. Adachi, S. Souda and I. Saito, *J. Med. Chem.*, 1994, **37**, 2106–2111.
- 21 N. Rahmannejadi, S. Khabnadideh and I. Yavari, *Monatsh. Chem.*, 2018, **149**, 2085–2092.
- 22 N. Rahmannejadi, I. Yavari and S. Khabnadideh, *J. Heterocycl. Chem.*, 2020, **57**, 978–982.
- 23 R. A. Castaldo, D. W. Gump and J. J. McCormack, *Antimicrob. Agents Chemother.*, 1979, **15**, 81–86.
- 24 J. H. Chan, J. S. Hong, L. F. Kuyper, D. P. Baccanari, S. S. Joyner and R. L. Tansik, *et al.*, *J. Med. Chem.*, 1995, **38**, 3608–3616.
- 25 N. Rahmannejadi, K. Zomorodian, Z. Faghieh, Z. Faghieh and S. Khabnadideh, *J. Pharm. Res. Int.*, 2017, 1–11.
- 26 J. Hanusek, *Chem. Listy*, 2001, **95**, 811–813.
- 27 L. Kubicova, P. Kudelova, H. Dostal and K. Waisser, *Folia Pharm. Univ. Carol.*, 2000, **25**, 81–87.
- 28 M. Divar, K. Zomorodian, S. Bastan, S. Yazdanpanah and S. Khabnadideh, *Information Management*, 2018, **15**, 1457–1466.
- 29 M. Yen, J. Sheu, I. Peng, Y. Lee and J. Chern, *J. Pharm. Pharmacol.*, 1996, **48**, 90–95.
- 30 B. Lam, Z. Zhang, J. A. Stafford, R. J. Skene, L. Shi and S. L. Gwaltney II, *Bioorg. Med. Chem. Lett.*, 2012, **22**, 6628–6631.
- 31 J.-U. Peters, S. Weber, S. Kritter, P. Weiss, A. Wallier and M. Boehringer, *et al.*, *Bioorg. Med. Chem. Lett.*, 2004, **14**, 1491–1493.
- 32 S. R. Sagar, J. K. Agarwal, D. H. Pandya, R. P. Dash, M. Nivsarkar and K. K. Vasu, *Bioorg. Med. Chem. Lett.*, 2015, **25**, 4428–4433.
- 33 M. Boehringer, H. Fischer, M. Hennig, D. Hunziker, J. Huwyler and B. Kuhn, *et al.*, *Bioorg. Med. Chem. Lett.*, 2010, **20**, 1106–1108.
- 34 Y. Miyamoto, Y. Banno, T. Yamashita, T. Fujimoto, S. Oi and Y. Moritoh, *et al.*, *J. Med. Chem.*, 2011, **54**, 831–850.
- 35 K. V. Parsa and M. Pal, *Expert Opin. Drug Discovery*, 2011, **6**, 855–869.
- 36 J. Peters, S. Weber, S. Kritter, P. Weiss and A. Wallier, *Bioorg. Med. Chem. Lett.*, 2004, **14**, 1491–1493.
- 37 M. B. Wallace, J. Feng, Z. Zhang, R. J. Skene, L. Shi and C. L. Caster, *et al.*, *Bioorg. Med. Chem. Lett.*, 2008, **18**, 2362–2367.
- 38 Z. Zhang, M. B. Wallace, J. Feng, J. A. Stafford, R. J. Skene and L. Shi, *et al.*, *J. Med. Chem.*, 2011, **54**, 510–524.
- 39 L. Emami, R. Sabet, A. Sakhteman and M. Khoshneviszadeh, *J. Pharm. Res. Int.*, 2019, 1–15.
- 40 M. Fereidoonnehad, Z. Faghieh, A. Mojaddami, Z. Rezaei and A. Sakhteman, *Iran. J. Pharm. Res.*, 2017, **16**, 981.
- 41 M. Fereidoonnehad, H. A. Mirsadeghi, S. Abedanzadeh, A. Yazdani, A. Alamdarlou and M. Babaghasabha, *et al.*, *New J. Chem.*, 2019, **43**, 13173–13182.
- 42 Z. Faghieh, N. Rahmannejadi, R. Sabet, K. Zomorodian, M. Asad and S. Khabnadideh, *Results Pharm. Sci.*, 2019, **14**, 115.
- 43 H. R. Shahsavari, N. Giménez, E. Lalinde, M. T. Moreno, M. Fereidoonnehad and R. Babadi Aghakhanpour, *et al.*, *Eur. J. Inorg. Chem.*, 2019, 1360–1373.
- 44 P. Ramesh, D. Srinivasulu, D. Subbarao, K. Hemakumar, D. Rajasekhar and C. Nagaraju, *Pharm. Lett.*, 2012, **4**, 1344–1351.
- 45 S. Xu, Q. Hao, H. Li, Z. Liu and W. Zhou, *Org. Process Res. Dev.*, 2017, **21**, 585–589.
- 46 W. A. Weihofen, J. Liu, W. Reutter, W. Saenger and H. Fan, *J. Biol. Chem.*, 2005, **280**, 14911–14917.
- 47 D. K. Yadav, F. Khan and A. S. Negi, *J. Mol. Model.*, 2012, **18**, 2513–2525.
- 48 D. K. Yadav, S. Kumar, H. S. Saloni, M.-H. Kim, P. Sharma and S. Misra, *et al.*, *Drug Des., Dev. Ther.*, 2017, **11**, 1859.
- 49 C. Granchi, A. Capecchi, G. Del Frate, A. Martinelli, M. Macchia and F. Minutolo, *et al.*, *Molecules*, 2015, **20**, 8772–8790.
- 50 P. Chen, C. G. Caldwell, W. Ashton, J. K. Wu, H. He and K. A. Lyons, *et al.*, *Bioorg. Med. Chem. Lett.*, 2011, **21**, 1880–1886.
- 51 S. Iwata and C. Morimoto, *J. Exp. Med.*, 1999, **190**, 301–306.
- 52 K. Ohnuma, N. H. Dang and C. Morimoto, *Trends Immunol.*, 2008, **29**, 295–301.
- 53 D. Darmoul, M. Lacasa, L. Baricault, D. Marguet, C. Sapin and P. Trotot, *et al.*, *J. Biol. Chem.*, 1992, **267**, 4824–4833.
- 54 L. Vázquez-Iglesias, L. Barcia-Castro, M. Rodríguez-Quiroga, M. P. de la Cadena, J. Rodríguez-Berrocal and O. J. Cordero, *Biol. Open*, 2019, **8**, bio041673.